Evaluation of different turbulent combustion models based on tabulated chemistry using DNS of heterogeneous mixtures under multi-injection Diesel engine-relevant conditions

Eleftherios Gorgoraptis, Jean-Baptiste Michel, Stéphane Chevillard, Antonio Pires da Cruz

To cite this version:

Evaluation of different turbulent combustion models based on tabulated chemistry using DNS of heterogeneous mixtures under multi-injection Diesel engine-relevant conditions

Eleftherios Gorgoraptis · Jean-Baptiste Michel · Stéphane Chevillard · Antonio Pires da Cruz

Abstract This paper assesses the accuracy of partially-premixed turbulent combustion models based on the tabulation of chemical kinetics, under multi-injection Diesel engine-relevant conditions. For this purpose, 2-D direct numerical simulation (DNS) is carried out. Pockets of gaseous n-heptane are randomly distributed in a turbulent field of a partially burnt n-heptane/air mixture. The burnt gases composition and enthalpy correspond to the partial oxidation of a pilot injection that precedes the main injection, represented here by the fresh fuel pockets. The DNS domain is enclosed in a larger volume, permitting quasi-constant pressure autoignition. Chemical kinetics is modeled by a 29-species skeletal reaction mechanism for n-heptane/air mixture autoignition and flame propagation. A homogeneous isotropic turbulence spectrum is used to initialize the velocity field in the domain. A DNS database is generated varying the progress of the pilot injection combustion c_0 and the velocity fluctuation level u' of the turbulence spectrum. Three different modeling approaches are tested *a priori* against the DNS data: (1) the Tabulated Ho-

Eleftherios Gorgoraptis
IFP Energies nouvelles, 1 et 4 avenue de Bois-Préau 92852 Rueil-Malmaison, France ; Institut Carnot IFPEN Transports Energie,
now at Aramco Fuel Research Center, Aramco Overseas Company, 232 Avenue Napoléon Bonaparte 92852 Rueil-Malmaison, France

Jean-Baptiste Michel
IFP Energies nouvelles, 1 et 4 avenue de Bois-Préau 92852 Rueil-Malmaison, France ; Institut Carnot IFPEN Transports Energie
Tel. : +33 1 47 52 54 35
E-mail: jean-baptiste.michel@ifpen.fr (corresponding author)

Stéphane Chevillard
IFP Energies nouvelles, 1 et 4 avenue de Bois-Préau 92852 Rueil-Malmaison, France ; Institut Carnot IFPEN Transports Energie

Antonio Pires da Cruz
IFP Energies nouvelles, 1 et 4 avenue de Bois-Préau 92852 Rueil-Malmaison, France ; Institut Carnot IFPEN Transports Energie

mogeneous Reactor (THR), which is a direct exploitation of the chemistry tabulation ignoring any local mixture heterogeneity; (2) the Presumed Conditional Moment (PCM) model, which includes a separate statistical description for the mixture and the combustion progress; (3) the Approximated Diffusion Flame (ADF) model, which considers the heterogeneous turbulent reactor as a diffusion flame. Since the same chemical kinetics mechanism is used for the generation of the chemistry tabulation, the study is entirely focused on the evaluation of the different modeling assumptions. Results show that accounting for initial progress variable of the mixture (c_0) is mandatory for such models. They also indicate the omission of mixture fraction Z and progress variable c heterogeneities and the assumption of the statistical independence of Z and c as the main responsible for model discrepancies under the studied conditions.

1 Introduction

Compression-ignition engines are widely used, mainly due to their high thermal efficiency and consequent low CO_2 emissions compared to spark-ignition engines. However, this technology has some disadvantages related the limited control over autoignition of the air-fuel mixtures and heat release rate. Hence, in compression-ignition engines at their most basic form, the level of combustion noise and emissions of nitrogen oxides and particulate matter can become critical. An effective strategy to tackle these problems is to decompose fuel injection into multiple injection pulses permitting an optimal control of the fuel-air mixture formation and, thus, of the autoignition delay and the heat release rate. Multiple injection strategies, made possible by common rail (CR) injection systems, become more and more popular due to their advantages over conventional single injection cycles. The physical phenomena involved in such configurations, however, are complex and remain challenging. There is significant interaction between the mixture fields of the consecutive injections [1] and this interaction depends strongly on the injection timing [2]. The progress of multiple injection technology depends to a great extent on the more profound understanding of these mechanisms.

Recent progress in internal combustion engine technologies increasingly rely on computational fluid dynamics (CFD), which helps evaluating the most promising strategies at the preliminary stages of engine development. In order to offer the precision needed, CFD codes require the introduction of detailed chemical kinetics involving many species and chemical reactions to correctly simulate turbulent combustion over a wide range of operating conditions (fuel-air equivalence ratio, dilution rate, pressure, *etc.*). Transport equations for all the species and enthalpy could be solved in very refined meshes to capture in detail the effects of the turbulence-chemistry interaction. This approach is consistent but usually has as consequence high computational costs. With proper

simplifying assumptions, CFD modeling of combustion can be done without substantial compromise on the simulation accuracy, significantly reducing the CPU cost.

Until present, Reynolds-averaged Navier-Stokes (RANS) simulation of Diesel engines is performed with satisfactory results, using a variety of combustion models [3, 4]. In the case of multiple Diesel injections configurations, however, the use of the existing combustion models [5–7] either fails to correctly predict ignition delay, in-cylinder pressure evolution, heat release, *etc.* or comes at a computational cost that is not suitable for industrial applications. A promising modeling approach consists in the off-line generation of chemistry look-up tables based on simple computations (*e.g.* homogeneous reactors or laminar diffusion flames) using complex chemical schemes; the tabulations are then used in the CFD simulation, combined with turbulent combustion models, integrating the effects of detailed chemistry at a minimal CPU cost.

Several studies investigated the validity of such tabulated combustion models, either in academic geometries [8–12] or in the industrial context, relying on the comparison of the numerical simulation results with experimental data. These computations are strongly dependent on the choice of the detailed chemistry mechanism. It is therefore unsafe to draw conclusions on the predictive capacity of the tested models based on comparisons with experimental data, since it is impossible to determine whether the observed differences are due to modeling hypotheses or to chemical kinetics approximations. Pires da Cruz [13] and Chevillard *et al.* [3] followed a methodology for an *a priori* evaluation of turbulent combustion models, excluding any misleading influence of the chemical scheme; direct numerical simulation (DNS) was conducted using the same skeletal reaction mechanism implemented for the tabulated chemistry models. Therefore, the focus was exclusively put on the modeling assumptions. This methodology is applied in the present study for the evaluation and the extension of various tabulated combustion models on multi-injection Diesel engine-relevant conditions.

Previous DNS works have investigated autoignition phenomena in mixing layers under decaying turbulence. Mastorakos *et al.* [14] demonstrated that first ignition spots are localized in regions of the flow with low scalar dissipation rate χ and around a specific, "most reactive" value of mixture fraction Z_{MR}. These results, obtained with 2-D DNS with simplified methane chemistry at non-Diesel-relevant conditions, were later confirmed by following DNS works in high-pressure Diesel and Homogeneous Charge Compression Ignition (HCCI) engine-relevant configurations [15], including 3-D [16], and complex chemistry [17] studies.

Recent numerical works investigated two-stage ignition and negative temperature coefficient (NTC) regime, characteristic of many Diesel engine operating points. Mukhopadhyay and Abraham observed the impact of scalar dissipation rate χ on each of the two stages of the ignition process in laminar [18] and turbulent [19] mixing layers at Diesel-relevant conditions. Bansal *et al.* [20] and Luong *et al.* [21] conducted a parametric investigation of key variables such as composition and temperature stratification magnitude, tur-

bulence intensity, *etc.* and identified their impact on the ignition delay and heat release. Krisman *et al.* [22, 23] identified a diffusively-supported front of low-temperature chemistry (LTC) as a distinct combustion feature that affects the second stage of the ignition.

Useful insights have been obtained from the aforementioned DNS studies. However, analyses of the interaction of partially burnt gases with fresh fuel, corresponding respectively to separate injection phases in a multi-injection Diesel engine, remain limited. Given the prominence of this interaction, observed in Diesel injection-relevant experiments [1], further investigation of ignition and progress of combustion at these conditions is merited.

The present work reports the generation and the analysis of a 2-D DNS database covering a range of split Diesel injection-relevant conditions. These simulations serve as numerical experiments providing a model-free insight into the interaction between turbulent mixing and combustion chemistry when using multiple injection strategies. Three different models are put to the test by means of *a priori* comparison with the DNS results, indicating the best modeling assumptions and directing their prospective adjustment to multi-injection configurations.

The studied models are first summarized in Section 2. Section 3 is devoted to the description of the DNS configuration used in this study and the database generated. The *a priori* evaluation of the combustion models against this database is then presented and discussed in Section 4. Finally, Section 5 summarizes the key findings of the present study.

2 Description of studied turbulent combustion models

The progress of compression-ignition applications depends in large part on the capacity of the physical models to predict heat release rate and pollutant emissions. For this purpose, the effects of detailed chemistry need to be taken into account. This need, combined with a concerted effort for minimal computational cost, has led to the development of several methods for an *a priori* tabulation of chemistry, ready for use before launching CFD simulations. The basic idea is to generate look-up tables based on simple computations (*e.g.* homogeneous reactors or laminar diffusion flames) using complex chemical schemes, that are then used in CFD simulation, combined with a turbulent combustion model.

The chemistry tabulations used in this study relate the combustion quantities of interest (species mass fractions Y_k, temperature T, reaction rates $\dot{\omega}_{Y_k}$, *etc.*) to a mixture fraction Z and a progress variable Y_c, as in Flame Prolongation of ILDM[1] (FPI) [24] tabulation approach. Mixture fraction Z is a passive scalar characterizing local mixing, varying between 0 in pure air to 1 in pure fuel. Out of the various definitions of Z [25] for a fuel consisting entirely of carbon and hydrogen, the carbon and hydrogen atom conservation is retained here:

---

[1] Intrinsic Low Dimension Manifold

$$Z = \sum_{k \in \Omega} \frac{Y_k \, n_{C,k} \, m_C}{W_k} + \sum_{k \in \Omega} \frac{Y_k \, n_{H,k} \, m_H}{W_k} \tag{1}$$

where W_k refers to the molecular weight of the kth species, $n_{C,k}$, $n_{H,k}$ are the numbers of carbon and hydrogen atoms contained in the kth species molecule and m_C, m_H are the respective atomic masses. A mixture is called stoichiometric if the fuel-oxidizer ratio is such that both fuel and oxidizer are entirely consumed after combustion is completed.

The progress of combustion with respect to the equilibrium state, *i.e.* the transition between fresh reactants and fully burnt products can be represented by a progress variable Y_c. A possible definition of the progress variable for hydrocarbon combustion is based on CO and CO_2 mass fractions [26]:

$$Y_c = Y_{\text{CO}} + Y_{\text{CO}_2} \tag{2}$$

with the corresponding reaction rate:

$$\dot{\omega}_{Y_c} = \dot{\omega}_{Y_{\text{CO}}} + \dot{\omega}_{Y_{\text{CO}_2}} \tag{3}$$

Y_c^{eq} is the value of Y_c when the equilibrium state is reached (fully burnt gases), depending on equivalence ratio[2] and initial temperature. A normalized progress variable can thus be defined as:

$$c = \frac{Y_c}{Y_c^{\text{eq}}} \tag{4}$$

$c = 0$ corresponds to fresh reactants and $c = 1$ to fully burnt products.

In the context of industrial 3D RANS simulation, the resolved variables correspond to statistical averages. Each flow variable is decomposed into a mean and a fluctuating part using either Reynolds-averaging ($\overline{Q}$) or Favre-averaging (mass weighted averaging $\widetilde{Q}$). Mixture fraction Z is thus decomposed into a mass weighted mean $\widetilde{Z}$ and a fluctuating part Z''. Unmixedness, denoted $\widetilde{S_Z}$, can then be defined as following:

$$\widetilde{S_Z} = \frac{\widetilde{Z''^2}}{(\widetilde{Z} - Z_{\text{min}})(Z_{\text{max}} - \widetilde{Z})} \tag{5}$$

where Z_{min} and Z_{max} are the minimum and maximum values of mixture fraction, on the oxidizer and fuel stream, respectively. $\widetilde{S_Z}$ is equal to zero for a perfectly homogeneous mixture. In the following paragraphs, mean value and variance refer to a computational cell *e.g.* each cell of a RANS simulation, and TAB superscript refers to the corresponding tabulated values.

The studied models are based on the assumption that the statistical behavior of heterogeneous reacting turbulent mixtures can be described through probability density functions (PDFs) for Z and c. In its most basic form, the idea consists in considering a joint PDF of Z and c, denoted $\widetilde{P}(Z, c)$. Mean

---

[2] Ratio of the fuel-oxidizer ratio over the stoichiometric fuel-oxidizer ratio.

mass fractions $\widetilde{Y_k}$, reaction rates $\widetilde{\omega}_{Y_k}$, *etc.* are directly related to the respective tabulated values Y_i^{TAB}, $\dot{\omega}_{Y_k}^{\mathrm{TAB}}$, as shown below for the mean progress variable reaction rate $\widetilde{\omega}_{Y_c}$:

$$\widetilde{\omega}_{Y_c} = \int_{Z_{\min}}^{Z_{\max}} \int_{c_{\min}}^{1} \dot{\omega}_{Y_c}^{\mathrm{TAB}}(Z,c) \widetilde{P}(Z,c) \, \mathrm{d}Z \, \mathrm{d}c \tag{6}$$

DNS results can be post-processed to obtain the evolution of the joint probability density function $\widetilde{P}(Z,c)$. The latter can then be directly integrated over Z and c, as in Equation (6). This method does not in itself constitute a feasible modeling approach, since the sub-grid $\widetilde{P}(Z,c)$ is not available in the context of RANS simulation. It defines, nonetheless, the maximum precision to be expected by models built on the assumption of a direct relation of all quantities to a mixture fraction Z and a normalized progress variable c. The inputs and the assumptions of the three studied models are briefly described below.

2.1 THR

The Tabulated Homogeneous Reactor (THR) approach directly uses tabulated values without any additional modeling to describe the influence of heterogeneities of the mixture. All combustion quantities are therefore directly related to the respective tabulated values that correspond to the mean mixture fraction $\widetilde{Z}$ and the mean normalized progress variable $\bar{c}$, as shown below for $\widetilde{\omega}_{Y_c}$:

$$\widetilde{\omega}_{Y_c} = \dot{\omega}_{Y_c}^{\mathrm{TAB}}(\widetilde{Z},\bar{c}) \tag{7}$$

This approach can be seen as the equivalent of a direct integration of the chemical kinetics combined with chemistry tabulation. The interaction of the flow with chemistry below the grid level is ignored and combustion is supposed homogeneous at the level of the computational cell (RANS) or of the spatial filter (LES).

2.2 PCM

Vervisch *et al.* [8] proposed the Presumed Conditional Moment (PCM) model, in which the heterogeneities of the reacting mixture are taken into consideration through PDFs. Initially developed in the context of partially-premixed combustion, the PCM formalism was extended to turbulent self-ignited combustion by Galpin *et al.* [10]. In PCM, mixture fraction and normalized progress variable are assumed to be independent variables, allowing the joint PDF to be written as a product of two independent PDFs:

$$\widetilde{P}(Z,c) = \widetilde{P}(Z) \, \overline{P}(c) \tag{8}$$

Mean quantities of interest are calculated by integration of the independent PDFs product over Z and c.

Two different versions of the PCM approach are studied in the present work. In the first version, here referred to as "PCM-1", the fluctuations of the normalized progress variable are neglected and the normalized progress variable PDF is $\overline{P}(c) = \delta(c - \overline{c})$, where δ is the Dirac delta function. $\widetilde{P}(Z)$ can be approximated by a β distribution whose first and second moments are computed according to transport equations for mixture fraction mean $\widetilde{Z}$ and variance $\widetilde{Z''^2}$. The mixture fraction variance $\widetilde{Z''^2}$ is conveniently normalized by its theoretical maximum to define unmixedness, as in Equation (5). Model response is obtained as follows:

$$\widetilde{\dot\omega}_{Y_c} = \int_{Z_{\min}}^{Z_{\max}} \int_{c_{\min}}^{1} \dot\omega_{Y_c}^{\mathrm{TAB}}(Z, c)\beta(Z)\delta(c - \overline{c}) \, \mathrm{d}Z \, \mathrm{d}c \tag{9}$$

In the second version, referred to as "PCM-2", $\overline{P}(c)$ is approximated by a β distribution whose first and second moments are computed according to transport equations for $\overline{c}$ and $\overline{c'^2}$, still assuming statistical independence between Z and c. The normalized progress variable variance $\overline{c'^2}$ is conveniently normalized by its theoretical maximum to define a segregation factor $\overline{S_c}$, as for the unmixedness $\widetilde{S_Z}$, yielding:

$$\widetilde{\dot\omega}_{Y_c} = \int_{Z_{\min}}^{Z_{\max}} \int_{c_{\min}}^{1} \dot\omega_{Y_c}^{\mathrm{TAB}}(Z, c)\beta(Z)\beta(c) \, \mathrm{d}Z \, \mathrm{d}c \tag{10}$$

The THR approach can be seen as a zero-order PCM model in which $\widetilde{S_Z}$ and $\overline{S_c}$ are equal to zero, or:

$$\widetilde{\dot\omega}_{Y_c} = \int_{Z_{\min}}^{Z_{\max}} \int_{c_{\min}}^{1} \dot\omega_{Y_c}^{\mathrm{TAB}}(Z, c)\delta(Z - \widetilde{Z})\delta(c - \overline{c}) \, \mathrm{d}Z \, \mathrm{d}c \tag{11}$$

2.3 ADF

The following briefly describes the Approximated Diffusion Flames (ADF) model; for further details, the reader is referred to the article by Michel *et al.* [27]. The ADF model is based on the approximation of 1-D diffusion flames in a counterflow configuration; Peters' flamelet Equation (12) is solved for the progress variable Y_c, from the pure mixing state to the equilibrium state, extracting directly the source term $\dot\omega_{Y_c}^{\mathrm{TAB}}$ from the look-up table.

$$\frac{\partial Y_c^{\mathrm{ADF}}}{\partial t} = \dot\omega_{Y_c}^{\mathrm{TAB}}\left(Z, \frac{Y_c^{\mathrm{ADF}}}{Y_c^{\mathrm{eq}}(Z)}\right) + \chi(Z, a)\frac{\partial^2 Y_c^{\mathrm{ADF}}}{\partial Z^2} \tag{12}$$

This approach has very low CPU requirements compared to the computation of an unsteady diffusion flame, as in Representative Interactive Flamelet (RIF) modeling [28], regardless of the complexity of the detailed chemistry

mechanism, thanks to the tabulation of $\dot{\omega}_{Y_c}^{\text{TAB}}$. The scalar dissipation rate χ is modeled as follows:

$$\chi(Z, a) = a\, \mathcal{F}(Z) \tag{13}$$

where a is the strain rate of the approximated diffusion flame, and $\mathcal{F}(Z)$ is a classical expression for counterflow diffusion flames [29]. A library of approximated flamelets is built resolving the Equation (12) for various strain rates a, using combustion chemistry in tabulated form. This library gives access to the evolution of the equivalent progress variable $Y_c^{\text{ADF}}(Z, a, t)$ and consequently to $\dot{\omega}_{Y_c}^{\text{ADF}}(Z, a, t) = \partial Y_c^{\text{ADF}}(Z, a, t)/\partial t$.

Once the approximate diffusion flames are calculated, integration is performed at each flamelet over PDFs of the mixture fraction Z. For this purpose, standardized β distributions are used, defined by the mixture fraction mean $\widetilde{Z}$, variance $\widetilde{Z''^2}$. Variance $\widetilde{Z''^2}$ is conveniently normalized to define unmixedness S_Z, as in Equation (5). Mean progress variable reaction rate $\widetilde{\dot{\omega}}_{Y_c}$ is thus obtained, taking into account both chemical and diffusive effects :

$$\widetilde{\dot{\omega}}_{Y_c}(\widetilde{Z}, Sz, a, t) = \int_{Z_{\min}}^{Z_{\max}} \frac{\partial Y_c^{\text{ADF}}}{\partial t}\beta(Z)\,\mathrm{d}Z \tag{14}$$

These quantities are finally written as functions of $\widetilde{Z}, S_Z, \widetilde{Y}_c$ and a using the bijective relation between time and mean progress variable and stored in a look-up table. Once the table has been generated, it can be read during the CFD calculation to obtain the tabulated values corresponding to the local values of $\widetilde{Z}, S_Z, \widetilde{Y}_c$ and a. These local values are obtained by transport equations.

It is noteworthy that, contrary to the PCM-2 approach, the shape of $\overline{P}(c)$ is not directly presumed in the ADF model. Nevertheless, $\overline{P}(c)$ can be estimated from tabulation inputs [27]. A progress variable value is attributed to each mixture fraction, so that the conditional PDF of the progress variable can be written as follows:

$$P(c|Z) = \delta(c - c^{\text{ADF}}(Z, at)) \tag{15}$$

Integration over mixture fraction Z allows to determine a progress variable PDF.

$$\widetilde{P}(c) = \int_{Z_{\min}}^{Z_{\max}} \widetilde{P}(Z)\delta(c - c^{\text{ADF}}(Z, at))\,\mathrm{d}Z \tag{16}$$

ADF can thus be seen as an extension of the PCM approach with the additional assumption of a diffusion flamelet structure correlating Z and c. The ADF model has been applied with success on autoigniting non-premixed jets [30] and single injection Diesel engines [4], coupled with the FPI tabulation approach.

3 DNS configuration, database and numerics

3.1 DNS configuration

3.1.1 Introduction of the physical problem

The lack of detailed experimental results of multiple injection combustion at the scale of interest orientates this study towards the use of DNS for the evaluation of the studied combustion models. DNS can provide a detailed insight into turbulent non-premixed combustion and is an excellent tool for model development [31].

In order to obtain an estimation of the conditions inside the combustion chamber of a typical automotive Diesel engine during autoignition, preliminary RANS simulations are conducted. For this purpose, the IFP-C3D code [32] is used and a double injection, low load and low engine speed operating point is chosen from a benchmark database validated against experimental data. The evolution of mean reaction rate $\bar{\dot{\omega}}$ and injected fuel mass m_{inj} for this operating point around top dead center (TDC) are presented in Figure 1(a). As can be seen, pilot injection initiates combustion just before TDC. Then, main injection is introduced, mixes with the ambient gases and quickly starts burning. In-cylinder pressure and temperature evolution over a larger part of the engine cycle are presented in Figure 1(b). Pressure when main injection fuel starts autoigniting is approximately 35 bar and temperature is around 890 K.
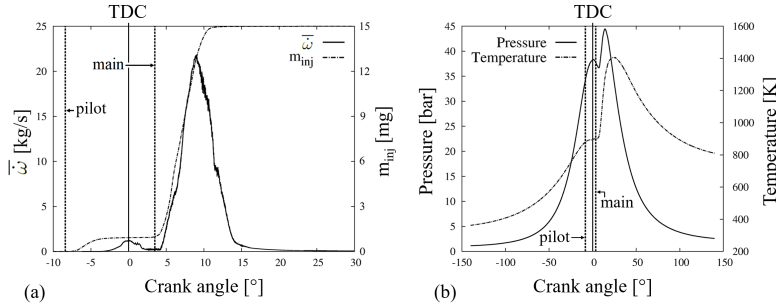

Fig. 1 RANS simulation of a double injection low load Diesel cycle (IFP-C3D). (a) Evolution of mean reaction rate $\bar{\dot{\omega}}$ and injected fuel mass m_{inj} around TDC, pilot injection and main injection timings. (b) Evolution of pressure and temperature over a part of the engine cycle.

Figure 2 illustrates instantaneous in-cylinder views of equivalence ratio and temperature fields for a sequence of times of this same operating point. Pilot injection is introduced, mixes with ambient air and autoignites. Main injection, starting approximately at 4° after TDC, is then introduced into areas where the combustion process is ongoing. This interaction between pilot

and main injection fields raises an important issue for combustion models based on tabulated chemistry, that needs to be examined: progress variable related to an initial state of fresh fuel-air mixtures can no longer be valid for mixtures of fresh fuel with burnt gases, even at identical equivalence ratio, temperature and pressure.
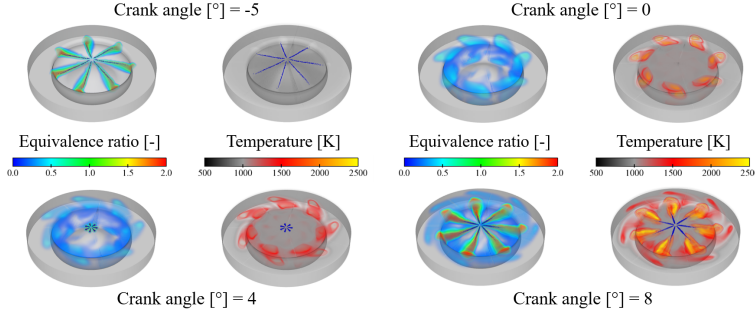

Fig. 2 RANS simulation of a double injection low load Diesel cycle (IFP-C3D); instantaneous in-cylinder views of equivalence ratio and temperature fields for a sequence of times.

3.1.2 Chemical kinetics mechanism

n-Heptane (n-C_7H_{16}) is chosen as the fuel of this work since its cetane number (CN $\simeq$ 56) is rather close to that of typical Diesel fuels (CN $\simeq$ 50); it is therefore expected to present autoignition delays that are similar to those of Diesel surrogates. Additionally, it has been the subject of an extended bibliography including numerous chemical kinetics schemes. This fuel can exhibit both single-stage and two-stage ignition, depending on the initial thermodynamic conditions and demonstrates a negative temperature coefficient (NTC) behavior. The chemical kinetics mechanism chosen for this study is a skeletal mechanism for n-heptane/air mixture autoignition and flame propagation proposed by Patel *et al.* [33], henceforth called "ERC mechanism". The mechanism consists of 29 species and 52 reactions and was developed and validated for multi-dimensional HCCI engine combustion simulations, with particular emphasis on the prediction of the ignition delay in high pressures (40-50 bar). The mechanism contains reactions that account for fuel decomposition, low-temperature oxidation, high-temperature oxidation and post-oxidation. The kinetic constants of two reactions of the original mechanism are updated as presented in Table 1, according to latest literature [34, 35] and respecting the uncertainties proposed by the authors.

3.1.3 Composition and temperature stratification

In the framework of this study, injected fuel heterogeneities are represented by a number of superposed Gaussian distributions of gaseous fuel mass fraction.

R_1	CH_2O	+	·OH	=	HCO	+	H_2O
R_2	·CH_3	+	HO_2	=	CH_3O·	+	·OH

		A	β	Ea
R_1	original	5.563 E+10	1.095	-76.5
R_1	updated	3.430 E+09	1.180	-447.0
R_2	original	5.000 E+13	0.0	0.0
R_2	updated	6.800 E+12	0.0	0.0

Table 1 Updated constants for ERC mechanism chemical kinetics mechanism [33–35].

No initial mean flow is imposed and only gaseous phase is considered since the analysis of spray dynamics is beyond the scope of this work. This configuration is considered representative of mixtures sufficiently far from the injector tip, out of the liquid penetration range of a Diesel spray, as illustrated in the schematic Figure 3.
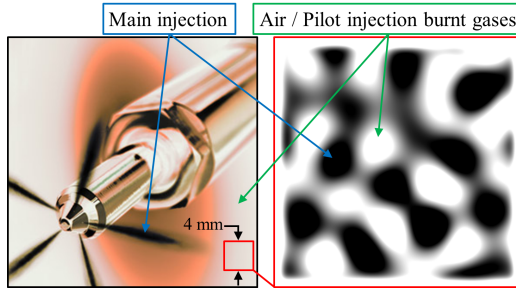

Fig. 3 Diesel injector fuel spray and composition stratification in the DNS configuration.

For the initialization of the composition fields of the DNS, adiabatic mixing of gaseous fuel and oxidizer streams is considered. The oxidizer stream can be pure air or pilot injection combustion products, depending on the case. Such mixing lines are schematically presented for a single and a split injection case in Figures 4(a) and (b), respectively. In the second case, pilot injection is mixing with air (mark A) and starts reacting before meeting the main injection. Combustion products, not necessarily at equilibrium, are computed in homogeneous reactor conditions (mark B), assuming that the pilot injection mixture is homogeneous. Thereafter, the DNS configuration is set up introducing a fuel mass fraction field inside an atmosphere of pilot injection combustion products. The initial composition at each node of the DNS domain is then found on the mixing line between pilot injection combustion products at Z_0 and maximum mixture fraction Z_{max} (mixing line B-C). In the following analysis, mixture fraction Z_0 and normalized progress variable c_0 refer to the homogeneous mixture representing the partially burnt gases of the pilot injection before mixing with the main injection fresh fuel in the split injection

cases. They correspond to different injection strategies and are key parameters in the present analysis since they are conditioning the initial composition and temperature stratifications of the DNS cases.
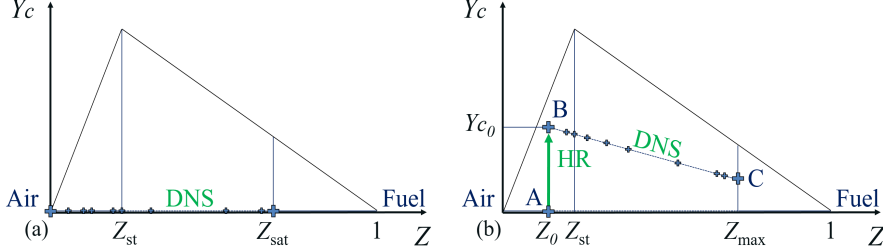

Fig. 4 Schematic view of DNS initialization for a single (a) and a split (b) injection case on $Y_c - Z$ mixing lines; pilot injection combustion products computed in homogeneous reactor (HR) (A-B), DNS initial conditions on mixing line B-C.

Considering a homogeneous mixture to represent the pilot injection is a strong assumption. Pitsch and Steiner [36] note that within the pilot injection stream of a piloted non-premixed methane-air diffusion flame (Sandia flame D) the mixture fraction gradient is zero. However, liquid fuel injection generally results in highly heterogeneous mixtures, even at high rail pressures. Assuming that pilot injection combustion products are homogeneous once they are reached by main injection fuel is relevant for injections which are not too close and for conditions resulting in relatively long pilot injection autoignition delays. In this scenario, pilot injection combustion is relatively slow compared to evaporation of the main injection. Pilot injection mixture field has thus the time to homogenize before burning or merging with the main injection mixture field. This is the case in the simulated double injection low load Diesel cycle illustrated in Figure 2. The limits of this assumption are reached for very close injections or very reactive conditions during pilot injection.

Figure 5 illustrates the temporal evolution of the normalized progress variable c in the homogeneous reactor that is relied upon to define the composition and temperature of the pilot injection partially burnt gases $Y_{k\,0}$ surrounding fresh (main injection) fuel pockets in the split injection cases. Its equivalence ratio is approximately 0.27 ($Z_0 = 0.0175$) and its initial temperature $T^{\text{init}} = 893$ corresponds to mark A on the mixing line illustrated in Figure 4(b). A two-stage ignition is clearly illustrated: the first increase of the normalized progress variable, corresponding to what is commonly called a cool flame, is followed by a plateau leading to the main ignition, at approximately 1.14 ms. The various progress variable c_0 levels of the DNS database are marked with coloured lines. Composition at $c_0 = 0.05$ corresponds to a mixture at cool flame ignition and $c_0 = 0.1$ is found in the midst of the cool flame. These mixtures contain large quantities of species participating in NTC and cool flame chemistry, with reactions accounting for fuel decomposition and low temper-

ature oxidation. $c_0 = 0.25$ is found right before main ignition and $c_0 = 0.5$ during main ignition, containing species participating in the ignition and high temperature oxidation process. $c_0 = 0.75$ mixture consists mainly of species that participate in high temperature oxidation and post-oxidation reactions. $c_0 = 1$ corresponds to fully burnt gases at the equilibrium state. All these different compositions are expected to behave very differently when mixed with fresh fuel, as discussed further on.
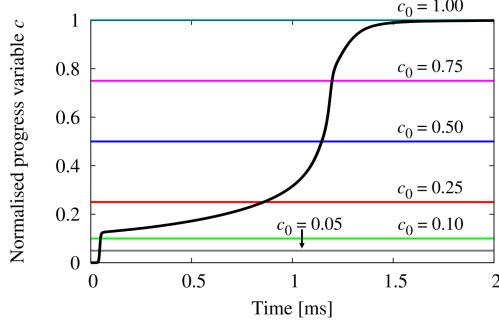

Fig. 5 Temporal evolution of normalized progress variable c of the pilot injection homogeneous mixture. The various c_0 levels of the split injection database marked with coloured lines.

The initial mean equivalence ratio ϕ is 1 for all DNS cases, that is $\widetilde{Z} = 0.062 = Z_{\text{st}}$ according to the definition of Equation (1). In single injection cases, Z_0 and c_0 are equal to zero and maximum mixture fraction is equal to an estimate of the saturation value of gas phase mixture fraction under the studied conditions $Z_{\text{sat}} = 0.5$. The choice of this value should not have a decisive impact on the outcome of this study, as demonstrated in an investigation of various maximum mixture fraction values in [3]. In real Diesel engines, droplet evaporation is limited by local vapor conditions and saturation value depends on ambient temperature and composition. Here, for the sake of simplicity, Z_{sat} is kept unchanged for all cases. In split injection cases, maximum mixture fraction Z_{max} is calculated according to the adiabatic mixing of a main injection stream at Z_{sat}, with a pilot injection burnt gases stream at Z_0, as in Equation (17) yielding $Z_{\text{max}} = 0.50875$.

$$Z_{\text{max}} = Z_{\text{sat}} + (1 - Z_{\text{sat}}) \, Z_0 \tag{17}$$

Fuel mass fraction stratification is initialized according to the following analytic expression:

$$Y_{\text{fuel}}^{\text{init}}(n) = f(n) \, Y_{\text{fuel 1}} + (1 - f(n) \, Y_{\text{fuel 1}}) \, Y_{\text{fuel 0}} \; , \;\; f(n) \in [0, 1] \tag{18}$$

$Y_{\text{fuel } 0}$ and $Y_{\text{fuel } 1} = Z_{\text{sat}}$ are the fuel mass fractions in the pilot and main injection streams, respectively. $Y_{\text{fuel}}^{\text{init}}(n)$ is then the total fuel mass fraction at every node n, as function of the respective value of the superposed Gaussian distributions $f(n)$ (see Figure 3). For the generation of these fields, the code the DNS code Asphodele [37] is used, as in [3], following the method of [38]. A maximum of $K_{\max} = 100$ components is used and maximum $f_{\max} = 1$ and mean $\mu = 0.133$ values are kept unchanged for all cases. As a result, the number of fresh fuel pockets is the same for all DNS cases. Variance σ^2 is adapted per DNS case to yield the same mass weighted mean $\widetilde{Z} = 0.062$ $= Z_{\text{st}}$. The resulting initial unmixedness $\widetilde{S_Z}$ values vary from 0.33 up to 0.54 depending on the case. These values indicate that the studied reactors are highly heterogeneous, in compliance with Diesel combustion. Mass fractions of the rest of the implicated 28 chemical species are then derived from the composition of pilot injection burnt gases stream $Y_{k\,0}$, as in Equation (19). It is redundant that in single injection cases $Y_{\text{fuel } 0}$ and $Y_{k\,0}$ are equal to zero and $Y_{k\,0}$ correspond to pure air composition.

$$Y_k^{\text{init}}(n) = (1 - Y_{\text{fuel}}^{\text{init}}(n))\, Y_{k\,0} \tag{19}$$

Initial temperature stratification is chosen to be correlated to the composition field, to mimic the droplet evaporation cooling effect, as following:

$$T^{\text{init}}(Z) = Z\, T^{\text{fuel}} + (1 - Z)\, T^{\text{oxi}} \tag{20}$$

T^{oxi} and T^{fuel} are the oxidizer and gaseous fuel initial temperatures, respectively. In split injection cases, T^{oxi} is equal to the adiabatic temperature of the homogeneous fuel-air mixture at Z_0 with initial temperature $T^{\text{init}} = 893$ K, burning up to $c = c_0$ at a constant pressure of 35 bars. Gaseous fuel temperature is chosen so that mean total enthalpy is the same for all the DNS cases. Initial temperature range is reported as per the DNS case in Table 2.

3.1.4 Turbulence characteristics

Similarly to previous DNS [39–42], decaying isotropic turbulence is superimposed on chemical species field. The Rogallo pseudo-spectral method [43] is used to initialize the velocity field based on a Passot-Pouquet turbulent kinetic energy spectrum function [44]. Turbulence is modeled in a very simple way considering a single value for length scale and velocity intensity so that the comparison between chemistry and turbulence effects is easy to quantify. Of course, further studies should include a more realistic turbulence spectrum.

The aforementioned simulated double injection low load Diesel operating point is processed to extract approximate values of kinetic energy k and dissipation rate ε. The evolution of their mean values is presented in Figure 6(a) over a part of the engine cycle. Combustion appears to have a strong impact on turbulence intensity. Kinetic energy increases after main injection autoignition since heat release induces strong flow accelerations. On the other hand, it diminishes due to the large changes in kinematic viscosity associated

with temperature increase. In order to obtain a rough estimation of the level of kinetic energy and its dissipation rate in the reactive zones inside the domain, conditional probability density functions (PDF) of $k|_{\dot{\omega}>0}$ and $\varepsilon|_{\dot{\omega}>0}$ are extracted during main injection autoignition. These PDFs are presented in Figure 6(b), along with the mean values of k and ε. Nevertheless, these are rough estimations providing an order of magnitude of the physical quantities in question.
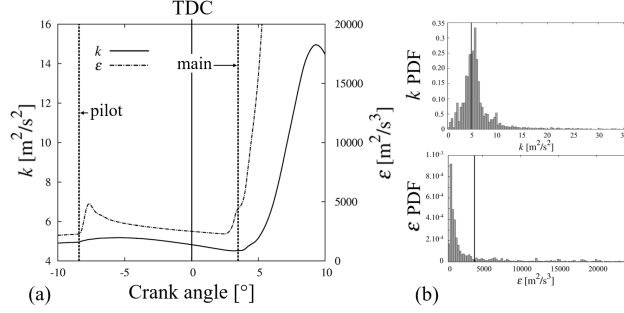

Fig. 6 RANS simulation of a double injection low load Diesel cycle (IFP-C3D). (a) Evolution of mean kinetic energy k and dissipation rate ε over a part of the engine cycle, pilot injection and main injection timings. (b) Conditional probability density functions of kinetic energy $k|_{\dot{\omega}>0}$ (left) and dissipation rate $\varepsilon|_{\dot{\omega}>0}$ (right) for positive values of reaction rate $\dot{\omega}$ and mean values (solid lines) during main injection autoignition.

Based on the indicative turbulence characteristics extracted from the RANS simulation, the velocity fluctuation u' during main injection autoignition is estimated at 1.8 m/s. Two levels of turbulence intensity are tested, 1.12 m/s and 5.60 m/s, respectively. The initial velocity field is assumed to be uncorrelated with composition and temperature fields. The integral length scale $l_t = k^{3/2}/\varepsilon$ estimate is of the order of a millimeter. The DNS domain should be a few times larger than l_t to provide converged statistics. A side length of 4 mm is thus chosen. Turbulent Reynolds number Re_t is chosen same for all cases and equal to 630, not far from the RANS simulation estimate $\simeq 700$. For this purpose, integral length scale l_t values are adapted per DNS case, to compensate viscosity changes for different c_0 values and the respective initial temperature range.

3.2 DNS database

A total of 12 DNSs are carried out by varying two parameters: (1) the progress of the pilot injection combustion c_0, and (2) the velocity fluctuations level u'. The objective is to study independently the effects of chemical progress and turbulent mixing, respectively. Cases a_0 and b_0 correspond to single injection strategies and have different velocity fluctuations levels u'. Cases a_1 - a_6 and

b_1 - b_4 correspond to different split injection strategies, varying c_0. A parameter study on pilot injection mixture fraction Z_0 would also be valuable to investigate the effect of the latter on the predictive capacity of the studied models. However, this work is limited to c_0 and u' variations, due to restricted computational resources. Initial unmixedness values, temperature stratification range and integral length scale values, discussed in the previous sections, are regrouped in Table 2 for all 12 DNS cases.

A main ignition delay τ_{AI} is defined as the time needed for the mean normalized progress variable to reach its median value, $i.e.$ $\tau_{\text{AI}} = t|_{\overline{c} = (c_{\min}+1)/2}$. Ignition delays are estimated for all DNS cases and are presented in Table 2. Turbulence time scales $\tau_t = k/\varepsilon$ and chemical time scales $\tau_c = 1/\widetilde{\omega}_{c\ \max}|_{Z=Z_{\text{st}}}$ are also estimated for all cases. According to these estimates, Damköhler number Da, comparing turbulent τ_t with the chemical τ_c time scales, varies between 25 and 1562, depending on the case.

Case	c_0	$\widetilde{S_Z}$	T^{init}	u'	l_t	τ_{AI}	τ_t	τ_c	Da
a_0	0.00	0.33	700 - 900	1.12	1.4	287	1052	1.7	621
a_1	0.05	0.39	701 - 942	1.12	1.4	329	947	1.7	549
a_2	0.10	0.41	702 - 967	1.12	1.6	430	1129	1.7	648
a_3	0.25	0.44	705 - 1034	1.12	1.8	338	1310	1.8	738
a_4	0.50	0.51	715 - 1158	1.12	2.2	59	1546	1.8	855
a_5	0.75	0.53	790 - 1350	1.12	2.7	23	1875	1.7	1102
a_6	1.00	0.54	818 - 1537	1.12	3.4	17	2419	1.5	1562
b_0	0.00	0.33	700 - 900	5.60	0.3	311	42	1.7	25
b_1	0.05	0.39	701 - 942	5.60	0.3	289	46	1.7	27
b_2	0.10	0.41	702 - 967	5.60	0.3	437	47	1.7	27
b_3	0.25	0.44	705 - 1034	5.60	0.4	335	52	1.8	30
b_4	0.50	0.51	715 - 1158	5.60	0.4	59	62	1.8	34
	[-]	[-]	[K]	[m/s]	[mm]	[µs]	[µs]	[µs]	[-]

Table 2 Physical parameters of the different cases.

3.3 DNS numerics

DNS is conducted using the compressible CFD code AVBP [45] which solves the time-dependent compressible Navier-Stokes equations for multi-species reactive flows in two and three space dimensions. The numerical scheme used is two-step Taylor-Galerkin (TTGC) [46], a third-order scheme barely dissipative and dispersive, therefore suitable for DNS [47, 48]. Diffusive terms are calculated with the Hirschfelder and Curtiss approximation [49].

For the purposes of this work, AVBP is coupled with the chemical kinetics solver CLOE (CLosed hOmogeneous rEactor) from the IFP-Kinetics package [50], developed and owned by IFPEN. Chemical kinetics are resolved at every

node of the mesh independently of diffusive and convective transport processes, as in a homogeneous reactor, what is known as the Operator-Splitting technique [51]. Chemical source terms and therefore the change in composition that corresponds to chemical reactions at every time-step are obtained using a first-order scheme. The implicit solver DVODE [52] is used for a robust resolution of the chemistry, even in the case of very stiff chemical kinetics.

As the characteristic time of autoignition in Diesel engines is small compared to that of the pressure evolution, pressure can be considered locally quasi-constant during the beginning of autoignition. Consequently, a constant pressure DNS set-up is preferred. A periodic domain, commonly used in DNS, would restrict the study to a constant volume configuration. Preliminary tests showed that undesirable acoustic phenomena are amplified in a small periodic domain. More specifically, pressure waves generated by autoignition overlap while exiting and re-entering the domain through its periodic borders, creating high frequency modes that are not representative of the problem of interest. This effect is even more present at high pressures. For these reasons, the DNS domain containing the reactive mixture is enclosed in a larger domain filled with air or pilot injection partially burnt gases, depending on the case (c_0, Z_0), as shown in Figure 7. The boundaries of the domain are all set to be adiabatic and free-slip. Combustion chemistry is only used within the DNS domain and the outer domain is non-reactive. The expansion of the burnt gases inside the DNS domain is small compared to the volume of the outer domain. This approach allows autoignition simulation under quasi-constant pressure, including the local flame generated density fluctuations and eliminating any undesirable acoustic phenomena. Computational cost is not penalized since the outer domain is discretized with a coarse mesh. The following analysis is limited to the central well refined DNS domain.
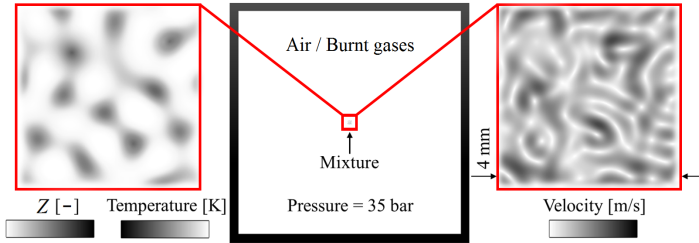

Fig. 7 Numerical configuration: initial mixture fraction, temperature (left) and velocity field (right). The larger outer domain (middle) allows constant pressure autoignition.

The resolution of all length and time scales in turbulent flow on high turbulent Reynolds number can be very demanding in terms of CPU cost. However, depending on the thermodynamic conditions and the chemical kinetics mechanism, the stiffness associated with the determination of rates of chemical reactions can be even more costly. A series of 1-D simulations with different grid resolutions is performed to asses the required resolution. The initial

species mass fraction and temperature profiles used correspond to a mixing layer of the same thickness as in the initial fields of cases a_0 and b_0 (c_0, $Z_0 = 0$). The tests are conducted under constant pressure of 35 bar. Ignition delay is found to depend on the resolution of the 1-D domain; grid convergence must therefore be sought. In Figure 8, ignition delay is plotted against the number of nodes in the reaction zone, here delimited by the hydroxyl radical peaks at its borders. Mesh independence is attained when these reaction layers are resolved with at least 25 grid points. This resolution corresponds to a mesh size Δx of 4 μm. This resolution is not necessarily sufficient as the mixing layers can be thinner than those in the initial conditions of the DNS due to the strain effect. Further studies should asses the required resolution for steeper gradients and in 2-D configurations. Nevertheless, the required resolution obtained from the 1-D configuration corresponds to 1000 grid points in each direction of the DNS domain. In view of values reported in Table 2, this resolution is also deemed adequate to provide converged statistics and to resolve all turbulent structures, from the biggest to the smallest. A 2-D configuration is adopted, as is the case for many contemporary DNS studies of autoignition [21–23, 39, 53, 54]. Although differences between 2-D and 3-D autoignition synopses are to be expected [16, 55], 2-D turbulent heterogeneous reactors remain relevant for the evaluation of model hypotheses. Nevertheless, further studies should investigate 3-D DNS results to confirm the presented observations.
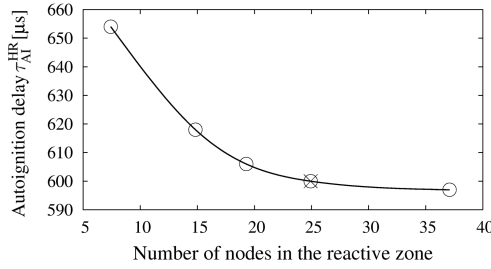

Fig. 8 Ignition delay against number of nodes in the reaction zone (circles) and chosen resolution (x mark), 1-D simulation.

4 Results and discussion

4.1 Phenomenological analysis

Figure 9 shows the ignition delay $\tau_{\mathrm{AI}}^{\mathrm{HR}} = t|_{c = (c_{\min}+1)/2}$ of homogeneous mixtures at 35 bar as a function of mixture fraction Z. Every curve is obtained by a series of 0-D homogeneous reactor calculations with the ERC mechanism [33], considering adiabatic mixtures of gaseous fuel and partially burnt gases streams for a value of c_0. Initial composition and temperature correlation is

kept same as in the respective DNS cases. The shortest ignition delays can be used as a reference to be compared with the ignition delays of stratified turbulent mixtures τ_{AI} reported in Table 2. These delays can be considered as the minimum possible for mixtures created by fuel and oxidant streams of the given initial temperatures [56]. These results should be taken with caution since the skeletal reaction mechanism [33] used was developed for n-heptane/air mixture autoignition and flame propagation under high pressure and with a certain level of exhaust gas recirculation (EGR), but has not been validated for fuel-partially burnt gases mixtures and for very rich mixtures ($\phi \simeq 16$ at $Z = Z_{\max}$). Nonetheless, the evaluation of the studied models presented in the following sections should not be largely impacted by this fact, since both DNS and tabulated chemistry models use the ERC mechanism [33].
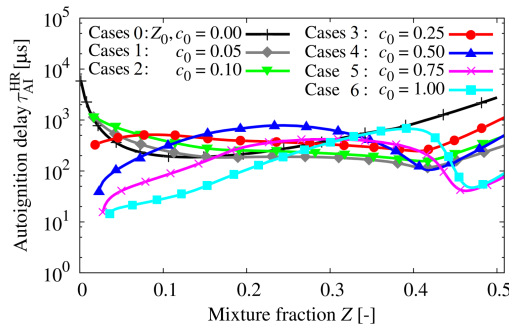
Fig. 9 0-D ignition delay $\tau_{\mathrm{AI}}^{\mathrm{HR}}$ of main injection fuel-pilot injection partially burnt gases homogeneous stoichiometric mixtures at 35 bar as function of mixture fraction Z, with Z dependent initial temperature using ERC mechanism [33].

The mixture fraction distributions $\widetilde{P}(Z)$ in the initial fields of DNS cases a_1 and a_6 are presented in figure 10. Combining the fact that the heterogeneous reactors are mostly lean (low Z) with the general tendencies of the 0-D ignition delay of Figure 9 and ignoring the decaying effect of turbulence and of temperature stratifications, a first indication of the reactivity of the heterogeneous reactors can be obtained. Cases a_4, b_4, a_5 and a_6 are expected to be much more reactive than cases a_1, b_1, a_2 and b_2, with much shorter chemical time scales τ_c and autoignition delays τ_{AI}.

The temporal evolution of the mean temperature $\widetilde{T}$ (left) and of the normalized progress variable $\bar{c}$ (right) of several DNS cases is presented in Figure 11. The reactivity of the heterogeneous reactors is found to present a multimode nature depending on c_0. Mixing partially burnt gases of $c_0 = 0.1$ with fresh fuel (green lines) gives reactors that autoignite slower than the equivalent fuel-air mixtures (black lines). Split injection cases a_3 and b_3 (red lines) present slightly longer ignition delays than single injection cases a_0 and b_0 (black lines). Once initiated, however, the combustion process advances faster
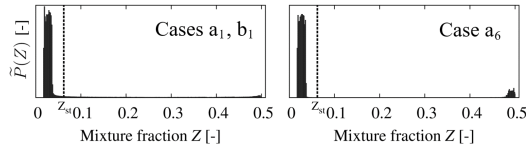
Fig. 10 Mixture fraction distributions $\widetilde{P}(Z)$ in the initial fields of DNS cases a_1, b_1 and a_6.

in these cases than in cases a_0 and b_0. Mixtures of cases a_4, b_4, a_5 and a_6 are very reactive and ignite almost instantaneously, regardless of the turbulent flow, and that is the reason of their exemption from the figure.
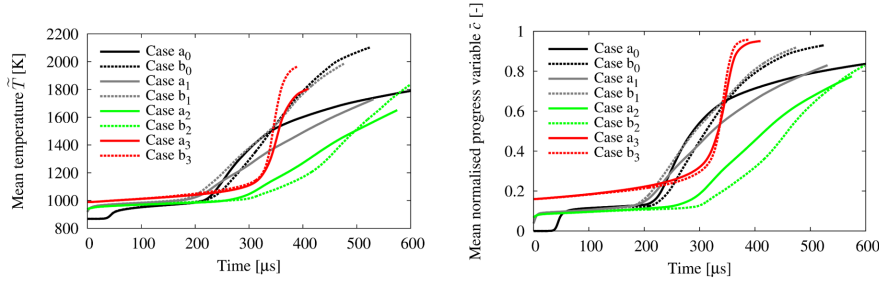

Fig. 11 Temporal evolution of mean temperature $\widetilde{T}$ (left) and mean normalized progress variable $\bar{c}$ (right) of several DNS cases.

The Damköhler number Da estimates presented in Section 3.2 and regrouped in Table 2 vary between 25 and 1562, depending on the DNS case. The laminar flamelet concept, viewing the turbulent diffusion flame as an ensemble of laminar diffusion flamelets [57], is only valid for high Damköhler numbers. This means that in some cases (where $Da \simeq 1$) the internal structure of the flame is potentially affected by turbulent mixing, whereas others (with $Da >> 1$), may be more propitious for flamelet modeling.

To highlight the differences between cases with higher and lower Damköhler number, cases a_3 and b_2, with $Da \simeq 738$ and $\simeq 27$, respectively, are chosen to be contrasted with one another. Mixture fraction Z and normalized progress variable c fields of DNS case a_3 are presented in Figure 12. Turbulence drives the formation of mixing layers and enhances heat transfer between hot, lean and cold, rich regions, leading to the main autoignition ($\bar{c} = 0.5$), arriving at 333 μs. Combustion progresses uniformly over a large range of Z: at $\bar{c} = 0.5$ few regions of the mixture have reached chemical equilibrium but most of them have started to react.

Figure 13 shows the evolution of mixture fraction Z and normalized progress variable c fields of DNS case b_2. Turbulent structures wrinkle strongly the mixture fraction field and strain the flame structures. Main ignition occurs at 459
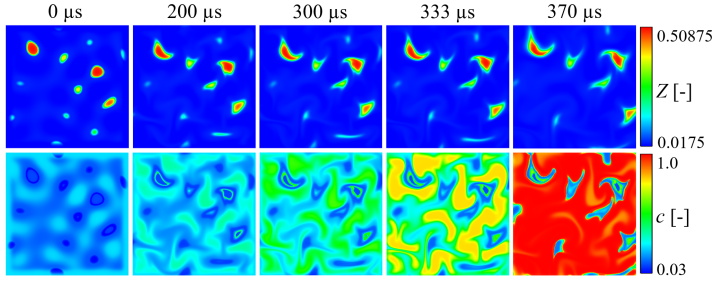
Fig. 12 Instantaneous views for a sequence of times; mixture fraction Z (first row) and normalized progress variable c (second row) fields of DNS case a_3.

µs. By contrast with case a_3, combustion progresses in a segregated way: at $\bar{c} = 0.5$ many regions of the heterogeneous mixture have already reached chemical equilibrium, whereas others have hardly started to react.
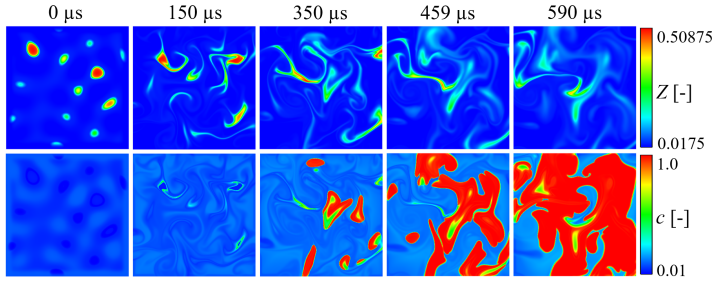

Fig. 13 Instantaneous views for a sequence of times; mixture fraction Z (first row) and normalized progress variable c (second row) fields of DNS case b_2.

When Damköhler number is assumed to be large, the burning rate can be quantified in terms of turbulent mixing. This assumption is only valid for combustion regimes where turbulence does not have an impact on the inner structure of the flame. In geometrical terms, this would mean that reaction zones' thickness is small compared to turbulent mixing length scales. Estimates of these length scales are proposed and compared for the DNS cases a_3 and b_2 at $\bar{c} = 0.7$. A reaction zone can be defined around every reaction rate peak, considering the thickness $\delta\dot{\omega}_c$ of the region in which reaction rate $\dot{\omega}_c$ values are higher than 10% of the peak. A turbulent mixing length scale δZ is defined based on the gradients of mixture fraction Z, as follows :

$$\delta Z = \frac{Z_{\max}^{\mathrm{loc}} - Z_{\min}^{\mathrm{loc}}}{|\nabla Z|} \tag{21}$$

where $Z_{\min}^{\mathrm{loc}}$ and $Z_{\max}^{\mathrm{loc}}$ are the local minimum and maximum values of a mixing layer within a chosen region of study. Fields of $|\nabla Z|$ and $\dot{\omega}_c$ of case a_3 at t

$= 350$ μs or $\bar{c} = 0.7$ are presented in Figure 14. A region combining a strong gradient of Z with a peak of $\dot{\omega}_c$ is found in the upper left corner of the DNS domain (red dashed circle). A line passing through the abscissa of this region is chosen (black dashed line). Values of $|\nabla Z|$ and $\dot{\omega}_c$ along this line are presented accompanied by values of Z (green line). According to the above definitions, estimated values $\delta\dot{\omega}_c = 58$ μm and $\delta Z = 100$ μm are calculated. According to these values, the thickness of this reaction zone is smaller than the mixing length scale.
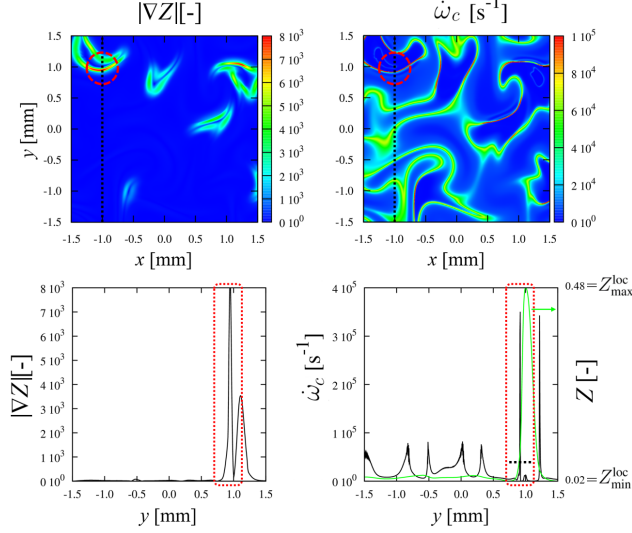

Fig. 14 Fields of $|\nabla Z|$ and $\dot{\omega}_c$ (upper figures), a region combining a strong gradient of Z with a peak of $\dot{\omega}_c$ (red dashed circle), a line passing through the abscissa of this region (black dashed line), and respective values of $|\nabla Z|$ and $\dot{\omega}_c$ along this line (lower figures) accompanied by values of Z (green line) for case a_3 at t $= 350$ μs or $\bar{c} = 0.7$.

The same procedure is repeated for case b_2. Figure 15 illustrates fields of $|\nabla Z|$ and $\dot{\omega}_c$ of this case at t $= 530$ μs or $\bar{c} = 0.7$. A region is again chosen (red dashed circle). Values of $|\nabla Z|$ and $\dot{\omega}_c$ on a line cutting through this region (black dashed line) are presented along with the distribution of Z (green line). The estimates obtained are $\delta\dot{\omega}_c = 20$ μm and $\delta Z = 20$ μm, meaning that the thickness of the reaction zone is of the same size as the mixing length scale. Hence, the internal structure of the flame is potentially affected by turbulent mixing.

This instantaneous comparison is not a complete demonstration allowing the classification of the two cases under different combustion regimes. It serves, nonetheless, as evidence for the interpretation of model response later on. Based on these observations, ADF model, which is based on the assumption of the flamelet structure, is expected to give more satisfactory results in case a_3 than in case b_2.
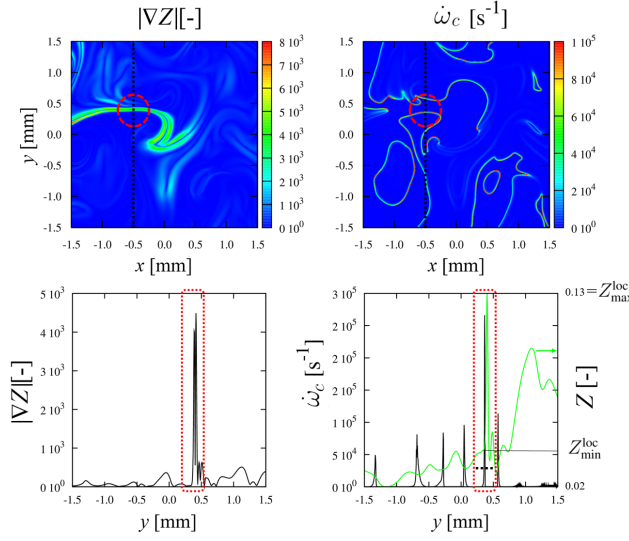
Fig. 15 Fields of $|\nabla Z|$ and $\dot{\omega}_c$ (upper figures), a region combining a strong gradient of Z with a peak of $\dot{\omega}_c$ (red dashed circle), a line passing through the abscissa of this region (black dashed line), and respective values of $|\nabla Z|$ and $\dot{\omega}_c$ along this line (lower figures) accompanied by values of Z (green line) for case b_2 at t = 530 μs or $\bar{c}$ = 0.7.

4.2 *A priori* model evaluation

The three modeling approaches presented in Section 2 are evaluated on the basis of an *a priori* comparison with the DNS results. The temporal evolution of mean values $\widetilde{Z}$ and $\bar{c}$, variances $\widetilde{Z''^2}$ and $\overline{c'^2}$, *etc.* corresponding to local (cell) values of transported variables in a RANS computation, are obtained by post-processing of the DNS cases, with a temporal sampling rate of one DNS solution every microsecond. These values are then treated by a model testing tool returning the model response, *i.e.* mass fractions and reaction rates, that are finally compared with the corresponding averaged DNS results. This methodology allows an evaluation of the model predictivity and does not accumulate errors, since the model inputs are retrieved from DNS post-processing at every time-step of the model evaluation test (every microsecond). The chemistry tabulations, relating mass fractions and reaction rates to the mixture fraction Z and the normalized progress variable c, are generated with the CLOE [50] solver. Both DNS and tabulated chemistry models use the same skeletal reaction mechanism (ERC [33]); therefore, the focus is exclusively put on the modeling assumptions. The evaluation of the models is based on the evolution of mean reaction rate of the progress variable $\widetilde{\dot{\omega}}_{Y_c}$ is presented, permitting to investigate the expected model behavior in terms of autoignition delay and heat release in the context of CFD engine simulation.

4.3 Influence of pilot injection combustion

As discussed in Section 4.1, the reactivity of the heterogeneous reactors is found to present a multi-mode nature depending on the composition and temperature of the oxidizer surrounding fresh fuel pockets (see Figure 11). These different behaviors have an effect on the predictive accuracy of the the models.

First, the evolution of the mean reaction rate of the progress variable $\widetilde{\omega}_{Y_c}$ with the mean normalized progress variable $\bar{c}$ is presented in Figure 16(a) for the single injection DNS case a_0 ($Z_0 = c_0 = 0$). Averaged DNS results are compared with model response, accompanied by the results of the direct integration over Z and c of the joint probability density function $\widetilde{P}(Z,c)$, as in Equation (6). A 0-D homogeneous reactor tabulation is used; mass fractions and reaction rates of homogeneous mixtures autoigniting under constant pressure of 35 bar are tabulated, covering mixture fraction range $Z \in [0, 0.5]$, with the same initial temperature-mixture fraction $T^{\mathrm{init}}(Z)$ correlation as in the single injection DNS cases. The THR approach fails to predict the evolution of the combustion process. The cool flame reaction rate peak arrives prematurely in progress variable terms, and the maximum reaction rate is strongly overestimated. This kind of behavior would lead to highly overestimated heat release rates in the context of engine simulation. PCM-1, considering only the mixture fraction heterogeneity through a presumed β distribution, clearly overestimates $\widetilde{\omega}_{Y_c}$. PCM-2, taking into account the progress variable heterogeneity independently of the mixture fraction, is an improvement compared to PCM-1. It remains inaccurate, however, since it overestimates by a factor of 10 the mean reaction rate over the largest part of the combustion process. This behavior is consistent with previous results [3, 11]. ADF gives significantly better predictions during cool flame (first peak) and is able to follow the general trend of the evolution of combustion process, readily decreasing reactivity while approaching $\bar{c} = 1$. Although improved, $\widetilde{\omega}_{Y_c}$ remains overestimated over a large part of the test.
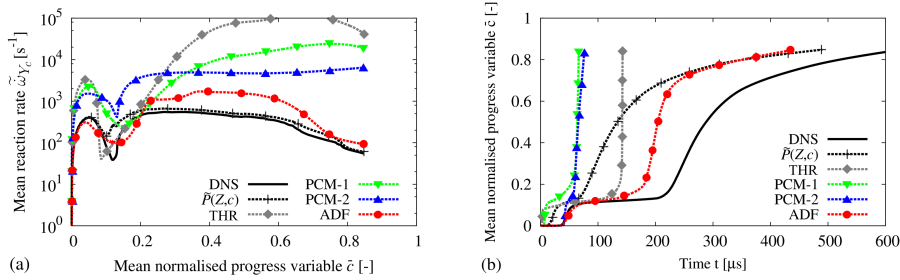

Fig. 16 Comparison between DNS results (solid lines) and evaluated models (dashed lines) using 0-D homogeneous reactor tabulation of fuel-air mixtures for single injection case a_0. (a) Evolution of mean reaction rate of the progress variable $\widetilde{\omega}_{Y_c}$ with mean normalized progress variable $\bar{c}$. (b) Temporal evolution of mean normalized progress variable $\bar{c}$.

In order to obtain estimations of autoignition delay predictions of the tested models, the above results are stored as functions of $\tilde{\dot{\omega}}_{Y_c}(\tilde{Y}_c)$ and integrated as following :

$$\tilde{\dot{\omega}}_{Y_c} = \frac{\partial \tilde{Y}_c}{\partial t} \Rightarrow t = \int \frac{1}{\tilde{\dot{\omega}}_{Y_c}} \mathrm{d}\tilde{Y}_c \tag{22}$$

Based on this approximation, a temporal evolution of $\overline{c}(t)$ is obtained for every studied model and presented in Figure 16(b). THR and PCM-1 models give a quasi-instantaneous cool flame ignition (first step in $\overline{c}(t)$ evolution) very far from the DNS results. A modeled main ignition delay can be defined as the time needed for this reconstructed mean normalized progress variable to reach its median value, *i.e.* $\tau_{\mathrm{AI}} = t|_{\overline{c} = (c_{\min}+1)/2}$. According to this criterion, PCM models underestimate autoignition delay by at least a factor of four. The THR approach gives a better estimation of autoignition delay, underestimating it by no more than a factor of two, but a very steep progress of combustion during main autoignition. ADF model gives more satisfactory results that are closer to the DNS progress variable evolution, and the most precise prediction of autoignition delay among the tested models, underestimating it by approximately 25%. The fact that, in terms of progress variable evolution, the ADF prediction is closer to the DNS than the direct integration of the joint probability density function $\tilde{P}(Z, c)$ can only be interpreted as a favorable accumulation of errors.

Cases a_1 - a_6 correspond to different split injection strategies (see Table 2), varying the progress of the pilot injection combustion c_0. Taking the example of split injection case a_3 ($c_0 = 0.25$), model response is compared to averaged DNS results in Figure 17(a). Here, the effect of c_0 on the combustion chemistry is omitted and a 0-D homogeneous reactor tabulation based on fuel-air mixtures is used. The ranking of the evaluated models in terms of accuracy is the same as in the single injection case presented above. However, all approaches give largely overestimated values of mean reaction rate. Even using the exact joint probability density function $\tilde{P}(Z, c)$, extracted directly from the DNS results, the modeled mean reaction rate does not follow the trend of the DNS at the beginning of the test. Based on the approximation of Equation (22), a reconstructed temporal evolution of the normalized progress variable $\overline{c}(t)$ is obtained for every studied model and presented in Figure 17(b) for case a_3. According to the aforementioned criterion $\tau_{\mathrm{AI}} = t|_{\overline{c} = (c_{\min}+1)/2}$, all evaluated models largely underestimate autoignition delay, by at least a factor of three.

The above discrepancies are due to the use of tabulated kinetics based on fuel-air mixtures, returning high reaction rate values for non-zero progress variable input. The behavior of mixtures of fuel with pure air can be very different from that of mixtures of fresh fuel with partially burnt gasses, even at identical Z and c. The progress variable related to an initial state of fresh fuel-air mixtures is no longer valid when multiple injections interact and a quantity of fresh fuel is injected into an area where the combustion process is ongoing. For this reason, 0-D homogeneous reactor tabulations are created
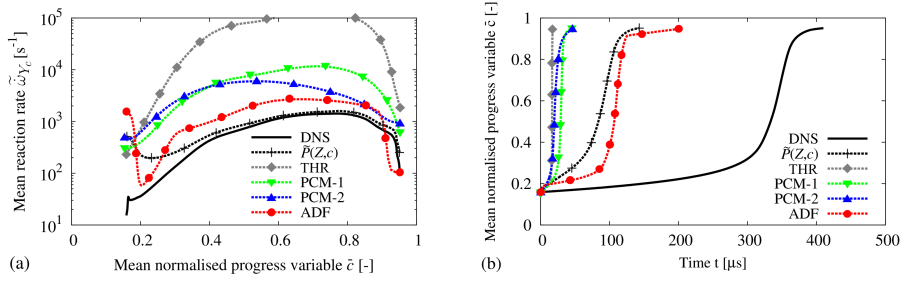
Fig. 17 Comparison between DNS results (solid lines) and evaluated models (dashed lines) using 0-D homogeneous reactor tabulation of fuel-air mixtures for split injection case a_3. (a) Evolution of mean reaction rate of the progress variable $\widetilde{\dot{\omega}}_{Y_c}$ with mean normalized progress variable $\bar{c}$. (b) Temporal evolution of mean normalized progress variable $\bar{c}$.

using adiabatic mixtures between a pilot injection burnt gases stream and a mixed pilot injection burnt gases-main injection fresh fuel stream (see Figure 4). The initial temperature-mixture fraction correlation $T^{\text{init}}(Z)$ is the same as in the respective DNS split injection cases (see Table 2). Six different split injection tabulations are generated, one for each tested value of c_0. Tabulated reaction rate of the progress variable $\dot{\omega}_{Y_c}^{\text{TAB}}$ values are shown in Figure 18 for cases a_0, b_0 ($Z_0 = c_0 = 0$) on the left, and cases a_3, b_3 ($Z_0 = 0.0125$, $c_0 = 0.25$) on the right, as an example.
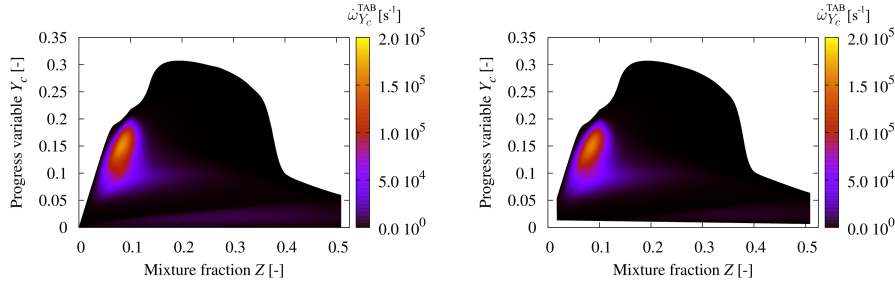

Fig. 18 0-D homogeneous reactor tabulation of reaction rate of the progress variable $\dot{\omega}_{Y_c}^{\text{TAB}}$ with mixture fraction Z and progress variable Y_c for cases a_0, b_0 ($Z_0 = c_0 = 0$) on the left, and cases a_3, b_3 ($Z_0 = 0.0125$, $c_0 = 0.25$) on the right.

The evolution of the joint probability density function $\widetilde{P}(Z, c)$ is obtained for all split injection cases by post-processing of the DNS results. $\widetilde{P}(Z, c)$ is then directly integrated as in Equation (6), using different tabulations. This method is repeated to cover the complete split injection database, testing all the available tabulations (one single injection and six split injection tabulations), so to unveil the impact of c_0 on the precision of PCM-type combustion models.

A relative error of the mean reaction rate of the progress variable $\widetilde{\dot{\omega}}_{Y_c}$ model predictions can be defined as:

$$\delta(\widetilde{\dot{\omega}}_{Y_c}) = \frac{\int |\widetilde{\dot{\omega}}_{Y_c}^{\mathrm{DNS}} - \widetilde{\dot{\omega}}_{Y_c}^{\mathrm{MODEL}}| \, \mathrm{d}\overline{c}}{\int \widetilde{\dot{\omega}}_{Y_c}^{\mathrm{DNS}} \, \mathrm{d}\overline{c}} \tag{23}$$

The relative error of the direct integration of $\widetilde{P}(Z, c)$ in the prediction of the mean reaction rate of the progress variable $\widetilde{\dot{\omega}}_{Y_c}$ is calculated for all cases and tabulations tested, according to the above definition. These values correspond to minimum discrepancies estimates for PCM-type models. Figure 19 regroups relative errors of the direct integration of $\widetilde{P}(Z, c)$ in the prediction of the mean reaction rate of the progress variable $\widetilde{\dot{\omega}}_{Y_c}$ using either a tabulation of fuel-air mixtures (TAB I) or an adapted tabulation (TAB II) generated as described above for each DNS case. The best agreement is systematically observed when using the adapted tabulation TAB II corresponding to the respective case. This analysis demonstrates the need for additional dimensions (c_0 and Z_0) on the tabulations used by the combustion models for multi-injection Diesel engine applications.
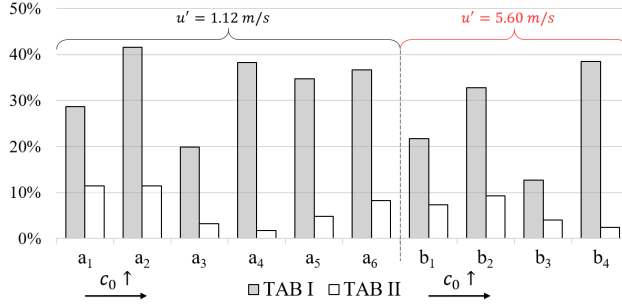

Fig. 19 Relative errors of the direct integration of $\widetilde{P}(Z, c)$ in the prediction of the mean reaction rate of the progress variable $\widetilde{\dot{\omega}}_{Y_c}$ using a fuel-air mixtures tabulation (TAB I) and adapted split injection tabulations (TAB II) for the corresponding DNS case.

Model predictions are recalculated for split injection case a_3 using the adapted tabulation based on fuel-burnt gases mixtures and are compared with the averaged DNS results in Figure 20(a). Discrepancies between the THR approach and the averaged DNS results remain very important, despite the adapted chemistry tabulation. The predictions of PCM and ADF models at the beginning of the test, however, are significantly ameliorated. The tendencies of the DNS results are approximately followed, with low reaction rate values for non-zero progress variable input and a reduction of reactivity while progress variable tends to unity. For PCM models, the maximum reaction rate is highly overestimated. The ADF model gives the best results among the tested models: it overestimates the small first peak of reactivity observed in the DNS and

then follows its evolution throughout the test. The relative error of the ADF prediction in this case is approximately 89%, as opposed to 123% of error using a tabulation corresponding to single injection cases, without taking into account Z_0 and c_0. Estimates of the temporal evolution of the normalized progress variable $\overline{c}(t)$ are presented in Figure 20(b) for the same case. The THR approach gives a very sharp quasi-instantaneous combustion. PCM models still strongly underestimate autoignition delay with approximately 75% of error. ADF gives the more satisfactory results with approximately 25% of error on the estimation of the autoignition delay. Once again, the fact that, in terms of progress variable evolution, the results of ADF are closer to the DNS than the direct integration of the joint probability density function $\widetilde{P}(Z,c)$ can only be interpreted as a favorable accumulation of errors.
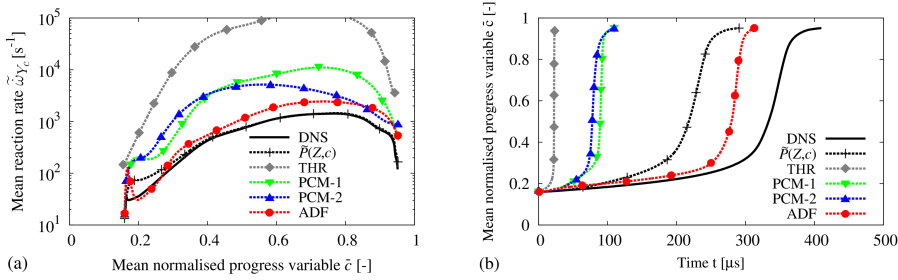

Fig. 20 Comparison between DNS results (solid lines) and evaluated models (dashed lines) using adapted 0-D homogeneous reactor tabulation for split injection case a$_3$. (a) Evolution of mean reaction rate of the progress variable $\widetilde{\omega}_{Y_c}$ with mean normalized progress variable $\overline{c}$. (b) Temporal evolution of mean normalized progress variable $\overline{c}$.

Model response compared to averaged DNS results are presented in Figure 21 for the low c_0 case a$_1$ ($c_0 = 0.05$). The THR approach, assuming a homogeneous mixture and making direct use of the chemistry tabulation, leads to overly inaccurate results in terms of reaction rate in this case. The THR prediction of the autoignition delay is interestingly close to the respective DNS results. However, the progress of combustion during the main ignition is extremely steep, unlike the DNS results. The two versions of the PCM model also give important discrepancies in the prediction of the mean reaction rate of the progress variable $\widetilde{\omega}_{Y_c}$, overestimating it by at least a factor of 10 over the largest part of the test. PCM-1, considering only the mixture fraction heterogeneity through a presumed β distribution, gives larger discrepancies in the prediction of the maximum $\widetilde{\omega}_{Y_c}$ values than PCM-2, taking into account the progress variable heterogeneity independently of the mixture fraction. However, PCM-1 is closer to the DNS than PCM-2 at the beginning of the test, resulting in a slightly better estimation of the autoignition delay. The ADF model gives the best results among the tested models: it predicts with good precision the first peak of mean reaction rate corresponding to cool flame reac-

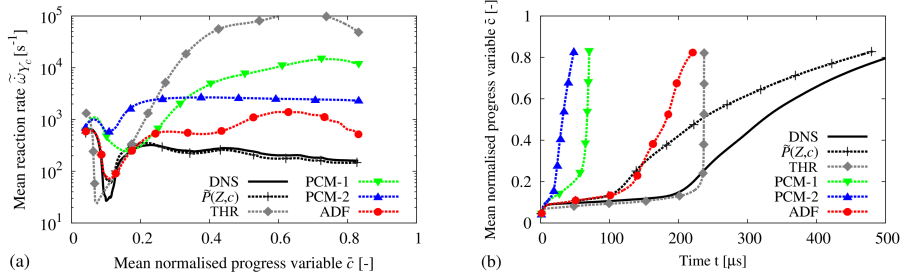tions, and generally gives the smallest discrepancies. These remarks also apply to case a_2.

Fig. 21 Comparison between DNS results (solid lines) and evaluated models (dashed lines) for split injection case a_1. (a) Evolution of mean reaction rate of the progress variable $\widetilde{\dot{\omega}}_{Y_c}$ with mean normalized progress variable $\bar{c}$. (b) Temporal evolution of mean normalized progress variable $\bar{c}$.

Model predictions compared to averaged DNS results are presented in Figure 22 for the higher c_0 case a_4 ($c_0 = 0.5$). The following observations also apply to cases a_5 and a_6. The THR model systematically overestimates the mean reaction rate by at least an order of magnitude and completely fails to predict its initial level for high c_0 values. PCM and ADF models, however, approximate the averaged DNS results with predictions that are substantially more precise, compared to low c_0 case a_1.
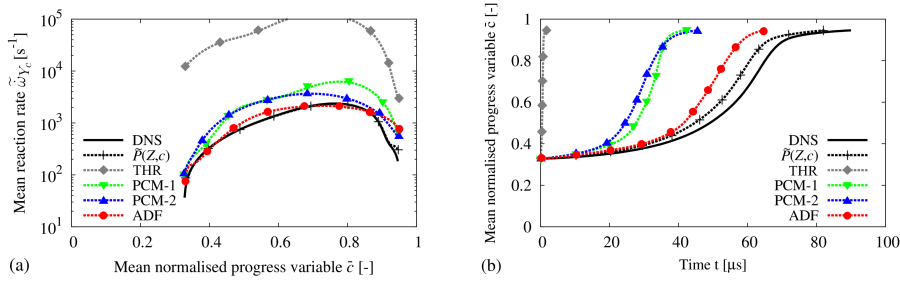

Fig. 22 Comparison between DNS results (solid lines) and evaluated models (dashed lines) for split injection case a_4. (a) Evolution of mean reaction rate of the progress variable $\widetilde{\dot{\omega}}_{Y_c}$ with mean normalized progress variable $\bar{c}$. (b) Temporal evolution of mean normalized progress variable $\bar{c}$.

Figure 23 regroups relative errors of the studied models over all low turbulence intensity split injection DNS cases a_1-a_6, estimated according to Equation (23). The ranking of the models in terms of mean reaction rate prediction accuracy is generally the same for all these cases, with THR model giving the

most inaccurate results, followed by PCM, and ADF model giving the smallest discrepancies among the tested approaches. Moving from lower to higher c_0 values, discrepancies are generally diminishing. A possible explanation for this may be that, as c_0 increases, especially over 0.5, the DNS cases become more reactive and the ignition process evolves increasingly faster, compared to the turbulent mixing, making the latter less important; the heterogeneous reactors then resemble more and more a conglomerate of homogeneous reactors and are more effectively modeled by the tabulated combustion models.
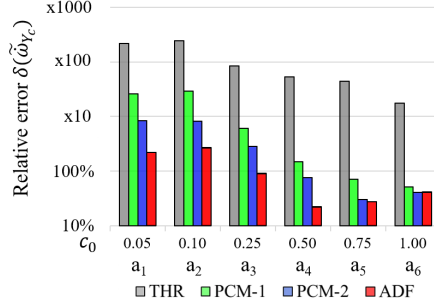

Fig. 23 Relative errors of the studied models in the prediction of the mean reaction rate of the progress variable $\widetilde{\omega}_{Y_c}$ for all low turbulence intensity split injection DNS cases with different values of c_0.

4.4 Influence of turbulence intensity

Two levels of turbulence intensity are tested, 1.12 m/s for a-cases, and 5.60 m/s for b-cases, respectively. Turbulent Reynolds number Re_t is chosen same for all cases and equal to 630. Integral length scale l_t values are chosen of the same order as the indicative value extracted from the preliminary RANS simulation, that is $\simeq 1$ mm, and so as to compensate viscosity changes for different c_0 values and the respective initial temperature range (see Table 2). Model predictions of the mean reaction rate of the progress variable $\widetilde{\omega}_{Y_c}$ of case a_2 are compared with those of case b_2 in Figure 24, for illustrative purposes.

The observed tendencies are verified over the complete DNS database. Figure 23 regroups the relative errors of the studied models, comparing lower turbulence intensity a-cases to higher turbulence intensity b-cases. THR model gives more accurate results in the high than in the low turbulence intensity cases. This may be explained by the fact that higher turbulence intensity leads to a more efficient turbulent mixing, resulting to faster homogenization. The hypothesis of homogeneity is therefore slightly better suited for the high turbulence intensity b-cases.

PCM model response is generally indistinguishable between the two groups. ADF model discrepancies are systematically higher in the high turbulence in-
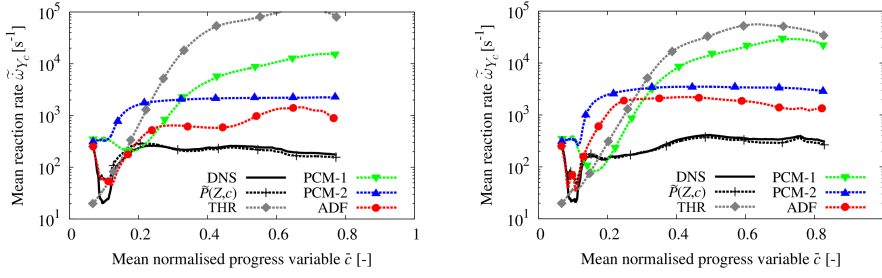
Fig. 24 Evolution of mean reaction rate of the progress variable $\widetilde{\omega}_{Y_c}$ with mean normalized progress variable $\bar{c}$; comparison between DNS results (solid lines) and evaluated models (dashed lines) for cases a_2 (left) and b_2 (right).
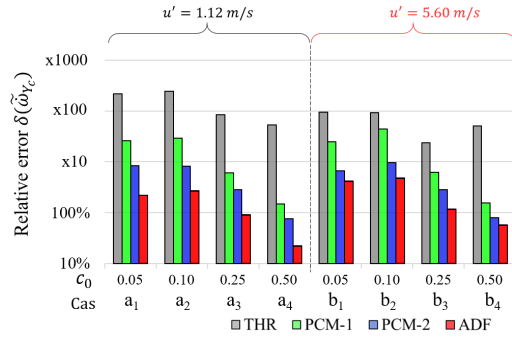

Fig. 25 Relative errors of the studied models in the prediction of the mean reaction rate of the progress variable $\widetilde{\omega}_{Y_c}$ for low turbulence intensity a-cases and high turbulence intensity b-cases.

tensity and low Da b-cases than in the low turbulence intensity and higher Da a-cases, as expected. Indeed, this model is based on the hypothesis that the turbulent heterogeneous reactor is composed of flammelets whose characteristic length and time scales are small compared to all turbulent scales. As discussed in Section 4.1, this hypothesis seems better adapted to low turbulence intensity cases.

4.5 Discussion over modeling assumptions

4.5.1 Influence of chemistry tabulation

The following analysis helps quantifying the part of the observed discrepancies between the evaluated combustion models and the DNS results that stems from the chemistry tabulation itself.

THR model response compared to averaged DNS results is presented in Figure 26 for single injection cases a_0 (left) b_0 (right). These results are accompanied by the response of a zero-order model, denoted here as "Arrhenius":

the DNS results are post-processed at every time-step of the model evaluation test (every microsecond) to obtain the mean mass fractions $\widetilde{Y_k}$ of all 29 chemical species transported. Then, chemical kinetics are resolved for one chemical time-step under constant pressure homogeneous reactor conditions, to obtain the reaction rate $\dot{\omega}_{Y_c}$ of this average composition. This test corresponds to a direct integration of chemical kinetics into the CFD simulation [58], without considering any interaction of the turbulent mixing with the chemical kinetics below the grid level. This is a quite popular approach that necessitates, however, the transport of as many additional variables as the species contained in the chemical kinetics mechanism and the parallel resolution of chemistry at every computational cell, demands that can drastically increase the CPU cost. The comparison of this method with the THR approach and the DNS results helps quantifying distinctively the part of the discrepancies that are due to the assumption of a homogeneous mixture and that of the tabulation of chemistry using 0-D reactors. At the beginning of the test, the biggest part of the observed error of the THR model can be attributed to the chemistry tabulation, since the Arrhenius approach is significantly closer to the averaged DNS results. Once the velocity field starts acting on the mixing process, however, discrepancies become important and the zero-order model approaches the THR results. These observations show that the homogeneous mixture assumption is an important source of error, especially when simulating highly heterogeneous mixtures.
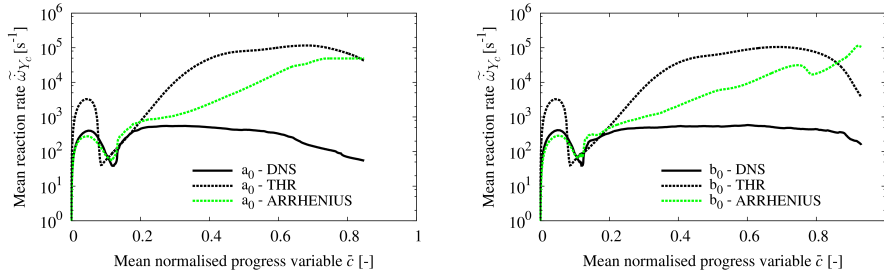

Fig. 26 Evolution of mean reaction rate of the progress variable $\widetilde{\dot{\omega}}_{Y_c}$ with mean normalized progress variable $\bar{c}$; comparison between DNS results (solid lines), THR approach (dashed black lines) and Arrhenius approach (dashed green lines), single injection cases a_0 (left) and b_0 (right).

As reported in Section 4.1, some of the reported DNSs present a relatively large Da number and therefore may be propicious for flamelet modeling. On the basis of this observation, a 1-D unsteady strained laminar diffusion flame tabulation is tested, similar to a flamelet-generated manifold (FGM) [59, 60], as in [61]. A constant strain rate a is chosen based on an estimated value during autoignition of the DNS case a_0, according to the following:

$$a = \frac{\widetilde{\chi}}{\int \mathcal{F}(Z)\widetilde{P}(Z)\,\mathrm{d}Z} \tag{24}$$

where $\mathcal{F}(Z)$ is the classical expression for counterflow diffusion flames [29]. The mean scalar dissipation rate $\widetilde{\chi}$ is a Favre-average of local $\chi = \mathcal{D}|\nabla Z|^2$ values.

Figure 27 illustrates a comparison between averaged DNS results and the direct integration of the joint probability density function $\widetilde{P}(Z,c)$ using either a 0-D homogeneous reactor tabulation (dashed black lines) or a 1-D unsteady strained laminar diffusion flame tabulation (dashed red lines), for single injection cases a_0 (left) and b_0 (right). This comparison highlights that the 1-D diffusion flame tabulation might be more suitable than the 0-D homogeneous reactor tabulation for the modeling of autoignition of such stratified turbulent mixtures. Discrepancies in case a_0 are less important than those of case b_0 in this test; this can be mainly attributed to the fact that the estimate of the strain rate a of the tabulated diffusion flame is based on case a_0 DNS results.
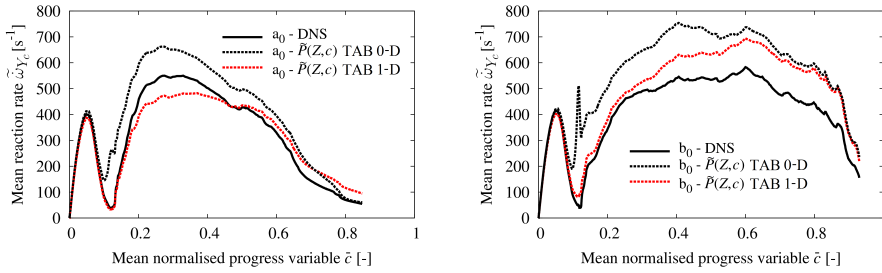

Fig. 27 Evolution of mean reaction rate of the progress variable $\widetilde{\omega}_{Y_c}$ with mean normalized progress variable $\bar{c}$; comparison between DNS results (solid lines) and the direct integration of the joint probability density function $\widetilde{P}(Z,c)$ using 0-D homogeneous reactor tabulation (dashed black lines), or 1-D unsteady strained laminar diffusion flame tabulation (dashed red lines), cases a_0 (left) and b_0 (right).

These results can be further improved using more adapted strain rate values that evolve in time. This methodology cannot be considered as a feasible modeling approach, since the joint $\widetilde{P}(Z,c)$ is not available in the context of RANS simulation; it defines, nonetheless, the maximum precision of combustion models using chemistry tabulations relating all quantities to mixture fraction Z and normalized progress variable c.

The evaluation of THR and PCM models was repeated using the 1-D unsteady strained laminar diffusion flame tabulation; the general tendencies of the models' response were similar and discrepancies with averaged DNS results remained important, indicating that a diffusion flame tabulation does not counterbalance the errors due to other model assumptions. Nevertheless,

the FPI-PCM and FGM approaches are equivalent in the present configuration.

The computation of unsteady diffusion flames during CFD runs, as in RIF [28] modeling, comes at a high CPU cost. An interesting alternative is the ADF [27] model, introducing a correlation of Z and c through the approximation of strained diffusion flames (see 2.3). DNS results are post-processed to obtain the evolution of strain rate a estimate; ADF tables are then generated, relating mean mass fractions $\widetilde{Y_i}$, reaction rates $\widetilde{\omega}_{Y_i}$, etc. to $\widetilde{Z}$, $\widetilde{S_Z}$, $\overline{c}$ and a, covering the range of strain rate values of interest. The response of this approach were presented in Sections 4.3 and 4.4.

4.5.2 Influence of Z and c statistical independence

To better understand the mismatch between the DNS and PCM-type models, statistical independence of Z and c is put to the test. Averaged DNS results (solid lines) are compared with the mean values obtained by direct integration of the independent probability density functions $\widetilde{P}(Z)$ and $\overline{P}(c)$ (dashed black lines), and of the joint probability density function $\widetilde{P}(Z,c)$ (dashed red lines) in Figure 28 for the single injection cases a_0 (left) and b_0 (right). The direct integration of the joint $\widetilde{P}(Z,c)$ gives a lot smaller discrepancies compared to the integration of the independent $\widetilde{P}(Z)$ and $\overline{P}(c)$ in both cases, as shown in [3] for similar single injection configurations.
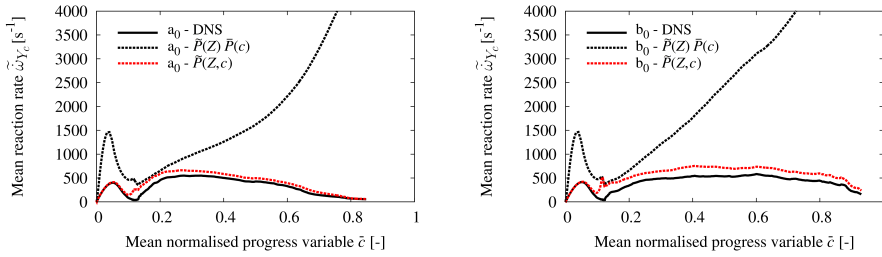

Fig. 28 Evolution of mean reaction rate of the progress variable $\widetilde{\omega}_{Y_c}$ with mean normalized progress variable $\overline{c}$; comparison between DNS results (solid lines), the direct integration of the independent $\widetilde{P}(Z)$ and $\overline{P}(c)$ (dashed black lines), and the direct integration of the joint $\widetilde{P}(Z,c)$ (dashed red lines) using 0-D homogeneous reactor tabulation, cases a_0 (left) and b_0 (right).

The same test is repeated for split injection cases a_3 and b_1 using adapted split injection tabulations and is presented in Figure 29. Again, direct integration of the joint $\widetilde{P}(Z,c)$ is much more accurate compared to the integration of the independent $\widetilde{P}(Z)$ and $\overline{P}(c)$ in both cases.

The relative errors in the prediction of the mean reaction rate of the progress variable $\widetilde{\omega}_{Y_c}$, using either the joint $\widetilde{P}(Z,c)$ or the independent $\widetilde{P}(Z)$
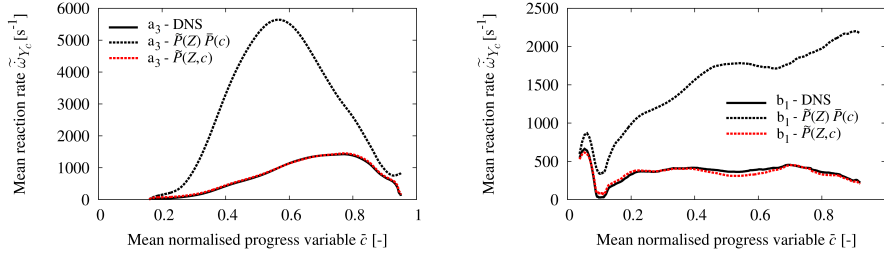
Fig. 29 Evolution of mean reaction rate of the progress variable $\widetilde{\omega}_{Y_c}$ with mean normalized progress variable $\overline{c}$; comparison between DNS results (solid lines), the direct integration of the independent probability density functions $\widetilde{P}(Z)$ and $\overline{P}(c)$ (dashed black lines), and the direct integration of the joint probability density function $\widetilde{P}(Z, c)$ (dashed red lines), cases a_3 (left) and b_1 (right).

and $\overline{P}(c)$ are calculated for all the split injection DNS cases and regrouped in Figure 30. According to these results, the assumption of the statistical independence can be assumed to be a major responsible for the discrepancies of the PCM model.
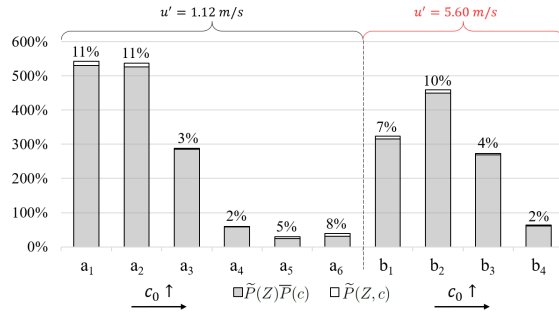

Fig. 30 Relative errors in the prediction of the mean reaction rate of the progress variable $\widetilde{\omega}_{Y_c}$ using either the joint $\widetilde{P}(Z, c)$ or the independent $\widetilde{P}(Z)$ and $\overline{P}(c)$, for all the split injection DNS cases.

4.5.3 Influence of PDF approximation

It was demonstrated that, in multi-injection configurations, taking into account the progress of the pilot injection c_0 in the chemistry tabulation improves significantly the model predictions. However, there are other possible sources of discrepancies to be understood and dealt with. The impact of the approximation of $\widetilde{P}(Z)$ and $\overline{P}(c)$ by presumed β distributions is investigated here.

This investigation reveals that the presumed $\beta(c)$ may fail if the kinetics include some stagnation of c, *e.g.* in the case of the cool flame, as reported

in [3]. This can be observed in Figure 31(a) comparing the actual $\overline{P}(c)$ with the presumed β distribution during cool flame (mark I) and main autoignition (mark II) in case a_0. DNS averaged results, PCM-2 prediction and the direct integration of $\overline{P}(c)$ for case a_0 are compared in Figure 31(b). Indeed, an important part of the model discrepancies can be attributed to the inaccurate approximation of the PDF of c by a β distribution. The accuracy of the standardized β distribution approximating the PDF of Z is found to be satisfactory. These tendencies are common for both single injection cases.
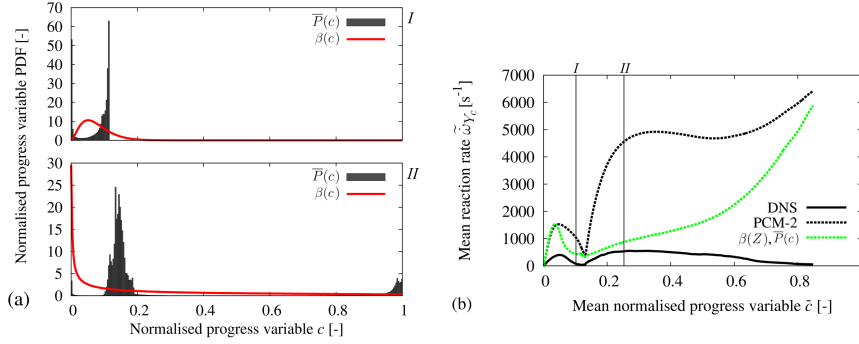

Fig. 31 (a) Comparison of the actual $\overline{P}(c)$ with the presumed β distribution during cool flame (mark I) and main autoignition (mark II) (b) Evolution of mean reaction rate of the progress variable $\widetilde{\omega}_{Y_c}$ with mean normalized progress variable $\bar{c}$; comparison between DNS results (solid line), PCM-2 model (dashed black line) and the direct integration of the $\overline{P}(c)$ (dashed green line), case a_0.

Similarly, a comparison between averaged DNS results (solid lines) and ADF model using either a standardized β distribution (dashed black line) or the actual $\widetilde{P}(Z)$ (dashed green line) is presented in Figure 32 for split injection case a_3. Indeed, an important part of the model discrepancies is due to the approximation of the PDF of Z by the β distribution. More specifically, when the evolution of the $\widetilde{P}(Z)$ is used, the relative error of the ADF model is reduced from 89% down to 26% for this case. Figure 32(b) reveals that the presumed $\beta(Z)$ may be insufficient if initial fields include some stagnation of Z, here right beyond Z_0.

The relative errors of the PCM and ADF models in the prediction of the mean reaction rate of the progress variable $\widetilde{\omega}_{Y_c}$, using either β distributions or the actual PDFs, are calculated for all the split injection DNS cases and regrouped in Figure 33. As can be observed, the inaccurate approximation of the PDFs contributes considerably to model discrepancies. PCM-2 model in case a_3 and ADF model in case a_4 give smaller discrepancies when using standardized β distributions instead of the actual PDFs. It should be noted that these results are most probably accidental in the sense that the accumulation of errors due to chemistry tabulation and the PDF approximation inadvertently lead to smaller relative errors.
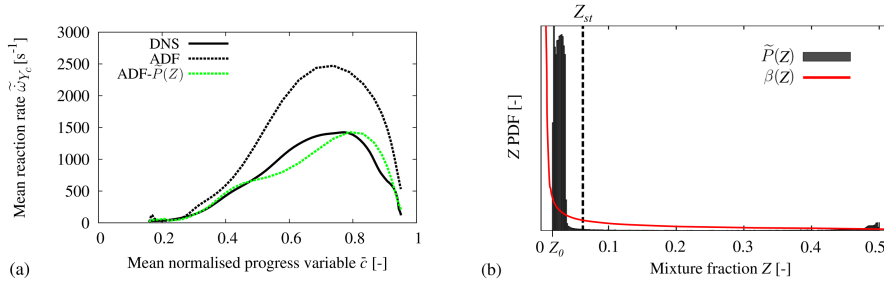
Fig. 32 (a) Evolution of mean reaction rate of the progress variable $\widetilde{\omega}_{Y_c}$ with mean normalized progress variable $\bar{c}$; comparison between averaged DNS results (solid lines) and ADF model using either a standardized β distribution (dashed black line) or the actual $\widetilde{P}(Z)$ (dashed green line) for split injection case a_3. (b) Comparison of the actual $\widetilde{P}(Z)$ with the presumed β distribution at the beginning of the test.
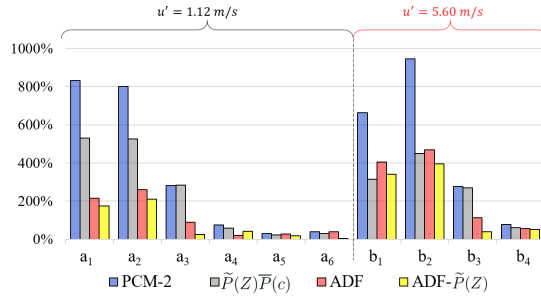

Fig. 33 Relative errors of the PCM and ADF models in the prediction of the mean reaction rate of the progress variable $\widetilde{\omega}_{Y_c}$, using either standardized β distributions or the actual PDFs, for all the split injection DNS cases.

A way to mitigate the part of the discrepancies that are due to the presumed β distributions could be to better adapt boundaries for the PDF integrals of Z and c. For example, a model could be added to better estimate maximum progress variable instead of always integrating up to $c = 1$. The reader is reffered to [62] for a thorough discussion on this subject. Furthermore, there exist alternatives for a more precise approximation of the PDFs, such as the presumed mapping function approach used in [63]. Their use in RANS simulation of multi-injection Diesel cycles can be an interesting perspective work.

5 Conclusions and perspectives

This study examined self-ignited combustion in turbulent heterogeneous reactors under multi-injection Diesel engine-relevant conditions, through DNS coupled with semi-detailed chemistry. The DNS configuration consists of segregated "main injection" fuel pockets randomly distributed within warm air

or partially "pilot injection" burnt gases, depending on the case, subjected to a turbulence field. A 2-D DNS database was generated and analysed, covering a range of single and split Diesel injection-relevant conditions. A parametric assessment was performed varying the progress of the pilot injection combustion c_0 and the velocity fluctuation level u' of the turbulence spectrum. The progress of combustion was found to present a multi-mode nature depending on c_0. Mixing partially burnt gases with fresh fuel can potentially give reactors that autoignite slower than equivalent fuel-air mixtures with same richness and total enthalpy. It can also result in mixtures presenting similar ignition delays with the fuel-air mixtures that advance faster once initiated. Finally, it can give very reactive heterogeneous reactors igniting much faster than fuel-air mixtures. An analysis of time and length scales of the DNS cases revealed that some of the studied cases (high c_0, low u', high Da) are more propitious for flamelet modeling than others (low c_0, high u', low Da).

The specific goal of this work was to evaluate turbulent combustion models based on tabulated chemistry and to elaborate a strategy to adapt them to the needs of modern multi-injection compression-ignition engine simulations. Three different modeling approaches were tested *a priori* against the DNS data: (1) the Tabulated Homogeneous Reactor (THR), which is a direct exploitation of the chemistry tabulation ignoring any local mixture heterogeneity; (2) the Presumed Conditional Moment (PCM) model, which includes a separate statistical description for the mixture and the combustion progress; (3) the Approximated Diffusion Flame (ADF) model, which considers the heterogeneous turbulent reactor as a diffusion flame. These modeling approaches are evaluated on the basis of an *a priori* comparison with the DNS database results. Since the same chemical kinetics mechanism is used for the generation of the chemistry tabulation, the study is entirely focused on the evaluation of different modeling assumptions. Key observations are summarized as follows :

- The ranking of the models in terms of mean reaction rate prediction accuracy was generally the same, with ADF model giving the smallest discrepancies among the tested approaches, followed by PCM and THR models. ADF thus appeared as the main candidate amongst the evaluated approaches for modern multi-injection compression-ignition engine simulation.
- Moving from lower to higher c_0 values, discrepancies were generally diminishing.
- THR model gave more accurate results in the high than in the low turbulence intensity cases.
- PCM model precision was generally indistinguishable between the low and high turbulence intensity u' cases.
- The assumption of statistical independence of mixture fraction Z and normalized progress variable c was found to be the main responsible for the discrepancies between averaged DNS and PCM results.
- The approximation of Z and/or c distributions by standardized β distributions can be imprecise, especially when kinetics include some stagnation

of c (*e.g.* cool flame) or Z_0 (*e.g.* pilot injection), leading to significant additional errors in the PCM and ADF models.
- ADF model discrepancies, were found systematically higher in the high u' and low Da cases than in the low u' and higher Da cases, in agreement with the analysis of time and length scales of the DNS results.
- Taking into account the effects of multiple injections (c_0 and Z_0) in the chemistry tabulation has proved to be an effective way of improving predictions of all the tested combustion models.

According to the above, existing models based on chemistry tabulation could be extended for the needs of modern multi-injection compression-ignition engine simulations by addition of dimensions in the look-up tables. The main limitation of this approach is expected to be the final table size, strongly impacting the precision of the simulation results. To overcome this problem, different approaches are possible: future work could be devoted to the use of neural networks or to the adaptation of the reduction techniques, as proposed in [64]. Alternatively, the additional dimensions could be limited to two, a mixture fraction Z_0 and a normalized progress variable c_0, to account for the partially burnt gases of previous injections interacting with new fuel feed regardless of the total number of injections, as in [7]. In this case, markers could be used in the CFD code to differentiate every injection event N from the $N-1$ injections preceding it. The partially burnt gases mixture fraction Z_0 surrounding fresh fuel in a computational cell could then be evaluated as the sum of the mixture fractions $\widetilde{Z}_n$ of the previous injections having reached the cell. The partially burnt gases normalized progress variable c_0 could be modeled as a function of the burnt fuel mass fraction of the partially burnt gases Y_{Fb}^0, evaluated as the sum of the progress variables of the previous $N-1$ injections, *e.g.* $c_0 = 1 - Y_{Fb}^0/Z_0$.

Conflict of interest

The authors declare that they have no conflict of interest.

References

1. G. Bruneaux, D. Maligne, Study of the mixing and combustion processes of consecutive short double Diesel injections, SAE Paper, 2009-01-1352 (2009).
2. Z. Han, A. Uludogan, G. Hampson, R. Reitz, Mechanism of soot and NOx emission reduction using multiple-injection in a Diesel engine, SAE Paper, 960633 (1996).

3. S. Chevillard, J.-B. Michel, C. Pera, J. Reveillon, Evaluation of different turbulent combustion models based on tabulated chemistry using DNS of heterogeneous mixtures, Combust. Theory Model. 21 (3) (2017) 440–465.
4. J.-B. Michel, O. Colin, A tabulated diffusion flame model applied to Diesel engine simulations, Int. J. Engine Res. 15 (3) (2013) 346–369.
5. N. Bordet, C. Caillol, P. Higelin, A physical 0d combustion model using tabulated chemistry with presumed probability density function approach for multi-injection Diesel engines, SAE Paper, 2010-01-1493 (2010).
6. C. Hasse, N. Peters, A two mixture fraction flamelet model applied to split injections in a DI Diesel engine, Proc. Combust. Inst. 30 (2005) 2755–2762.
7. C. Felsch, M. Gauding, C. Hasse, S. Vogel, N. Peters, An extended flamelet model for multiple injections in DI Diesel engines, Proc. Combust. Inst. 32 (2009) 2775–2783.
8. L. Vervisch, R. Hauguel, P. Domingo, M. Rullaud, Three facets of turbulent combustion modelling: DNS of premixed V-flame, LES of lifted nonpremixed flame and RANS of jet-flame, J. Turbul. 5 (2004) 1–36.
9. B. Fiorina, R. Vicquelin, P. Auzillon, N. Darabiha, O. Gicquel, D. Veynante, A filtered tabulated chemistry model for LES of premixed combustion, Combust. Flame 157 (3) (2010) 465–475.
10. J. Galpin, C. Angelberger, A. Naudin, L. Vervisch, Large-eddy simulation of H2-air auto-ignition using tabulated detailed chemistry, J. Turbul. 9 (2008).
11. J.-B. Michel, O. Colin, D. Veynante, Comparison of differing formulations of the PCM model by their application to the simulation of an auto-igniting H2/air jet, Flow Turbul. Combust. 83 (2009) 33–60.
12. J. Tillou, J.-B. Michel, C. Angelberger, D. Veynante, Assessing les models based on tabulated chemistry for the simulation of Diesel spray combustion, Combust. Flame 161 (2014) 525–540.
13. A. Pires da Cruz, T. Baritaud, Self-ingnition and combustion modeling of initially nonpremixed turbulent systems, Combust. Flame (2001) 65–81.
14. E. Mastorakos, T. Baritaud, T. Poinsot, Numerical simulations of autoignition in turbulent mixing flows, Combust. Flame 109 (1997) 198–223.
15. A. Viggiano, V. Magi, A 2-D investigation of n-heptane autoignition by means of direct numerical simulation, Combust. Flame 137 (2004) 432–443.
16. S. Sreedhara, N. Lakshmisha, Autoignition in a non-premixed medium: DNS studies on the effects of three-dimensional turbulence, Proc. Combust. Inst. 29 (2002) 2051–2059.
17. T. Echekki, J. Chen, Direct numerical simulation of autoignition in non homogeneous hydrogen-air mixtures, Combust. Flame 134 (2003) 169–191.
18. S. Mukhopadhyay, K. Abraham, Influence of compositional stratification on autoignition in n-heptane/air mixtures, Combust. Flame 158 (2012) 1064–1075.
19. S. Mukhopadhyay, K. Abraham, Influence of heat release and turbulence on scalar dissipation rate in autoigniting n-heptane/air mixtures, Combust. Flame 159 (2012) 2883–2895.

20. G. Bansal, A. Mascarenhas, J. Chen, Direct numerical simulations of autoignition in stratified dimethyl-ether (DME)/air turbulent mixtures, Combust. Flame 162 (2015) 688–702.
21. M. Luong, G. Yu, T. Lu, S. Chung, C. Yoo, Direct numerical simulations of ignition of a lean n-heptane/air mixture with temperature and composition inhomogeneities relevant to HCCI and SCCI combustion, Combust. Flame 162 (2015) 4566–4585.
22. A. Krisman, E. Hawkes, M. Talei, A. Bhagatwala, J. Chen, Characterisation of two-stage ignition in Diesel engine-relevant thermochemical conditions using direct numerical simulation, Combust. Flame 172 (2016) 326–341.
23. A. Krisman, E. Hawkes, M. Talei, A. Bhagatwala, J. Chen, A direct numerical simulation of cool-flame affected autoignition in Diesel engine-relevant conditions, Proc. Combust. Inst. (2016) 1–9.
24. O. Gicquel, N. Darabiha, D. Thevenin, Laminar premixed hydrogen/air counterflow flame simulations using flame prolongation of ildm with differential diffusion, Proc. Combust. Inst. 28 (2000) 2419–2425.
25. H. Pitsch, N. Peters, A consistent flamelet formulation for non-premixed combustion considering differential diffusion effects, Combust. Flame 114 (1998) 26–40.
26. B. Fiorina, R. Baron, O. Gicquel, D. Thevenin, S. Carpentier, N. Darabiha, Modelling non-adiabatic partially premixed flames using flame-prolongation of ildm, Combust. Theory Model. 7 (2003) 449–470.
27. J.-B. Michel, O. Colin, D. Veynante, Modeling ignition and chemical structure of partially premixed turbulent flames using tabulated chemistry, Combust. Flame 152 (2008) 80–99.
28. H. Barths, C. Hasse, G. Bikas, N. Peters, Simulation of combustion in direct injection Diesel engines using a Eulerian particle flamelet model, Proc. Combust. Inst. 28 (2000) 1161–1168.
29. N. Peters, Turbulent Combustion, Cambridge University Press, 2000.
30. J.-B. Michel, O. Colin, C. Angelberger, D. Veynante, Using the tabulated diffusion flamelet model ADF-PCM to simulate a lifted methane-air jet flame, Combust. Flame 156 (2009) 1318–1331.
31. H. Pitsch, P. Trisjono, Can combustion models be developed from DNS data?, 19th Australasian Fluid Mechanics Conference (2014) 350.
32. J. Bohbot, N.Gillet, A. Benkenida, IFP-C3D: an unstructured parallel solver for reactive compressible gas flow with spray, Oil Gas Sci. Technol. 64 (2009) 309 – 336.
33. A. Patel, S. Kong, R. Reitz, Development and validation of a reduced reaction mechanism for HCCI engine simulations, SAE Paper, 2004-01-0558 (2004).
34. D. Baulch, C. Cobos, R. Cox, C. Esser, P. Frank, Evaluated kinetic data for combustion modelling, J. Phys. Chem. Ref. Data 21 (1997) 411–429.
35. Z. Hong, D. Davidson, K. Lam, R. Hanson, A shock tube study of the rate constants of HO_2 and CH_3 reactions, Combust. Flame 159 (2012) 3007–3013.

36. H. Pitsch, H. Steiner, Scalar mixing and dissipation rate in large-eddy simulations of non-premixed turbulent combustion, Proc. Combust. Inst. 28 (1) (2000) 41–49.
37. J. Reveillon, C. Pera, Z. Bouali, Examples of the potential of DNS for the undestanding of reactive multiphase flows, Int. J. Spray Combust. Dyn. 3 (2011) 65–94.
38. J. Reveillon, Numerical procedures to generate and to visualize flow fields from analytical or experimental statistics: turbulent velocity, fluctuating scalars and variable density sprays, J. Flow Visualization Image Proc. 12 (2005) 1–19.
39. C. Pera, S. Chevillard, J. Reveillon, Effects of residual burnt gas heterogeneity on early flame propagation and on cyclic variability in spark-ignited engines, Combust. Flame 160 (2013) 1020–1032.
40. J. Hult, S. Gashi, N. Chakraborty, M. Klein, K. Jenkins, S. Cant, C. Kaminski, Measurement of flame surface density for turbulent premixed flames using PLIF and DNS, Proc. Combust. Inst. 31 (2007) 1319–1326.
41. T. Dunstan, K. Jenkins, Flame surface density distribution in turbulent flame kernels during the early stages of growth, Proc. Combust. Inst. 32 (2009) 1427–1434.
42. T. Dunstan, K. Jenkins, The effects of hydrogen substitution on turbulent premixed methane-air kernels using direct numerical simulation, Int. J. Hydrogen Energy 34 (2009) 8389–8404.
43. R. Rogallo, Numerical experiments in homogeneous turbulence, Tech. rep., technical Memorandum No. 81315 (1981).
44. T. Passot, A. Pouquet, Numerical simulation of homogeneous flows in the turbulent regime, J. Fluid Mech. (1987) 181–441.
45. T. Schoenfeld, The AVBP handbook, 2008.
46. O. Colin, M. Rudgyard, Development of high-order Taylor-Galerkin schemes for LES, J. Comput. Phys. 162(2) (2000) 338–371.
47. O. Cabrit, L. Artal, Direct numerical simulation of turbulent multispecies channel flow with wall ablation, 39th AIAA Thermophysics conference (2007) 4401.
48. F. Cadieux, J. Domaradzki, T. Sayadi, S. Bose, F. Duchaine, DNS and LES of separated flows at moderate Reynolds numbers, Center for Turbulence research, NASA Ames/Stanford University, Proceedings of the summer program (2012) 77–89.
49. J. Hirschfelder, C. Curtiss, R. Byrd, Molecular theory of gases and liquids, Vol. 26, Wiley New York, 1954.
50. A. Velghe, J. Bohbot, S. Jay, A high efficiency parallel architecture dedicated to internal combustion engine simulation coupled with chemical kinetic solver, 6th European Conference on Computational Fluid Dynamics (2014).
51. B. Sportisse, An analysis of operator splitting techniques in the stiff case, J. Comput. Phys. 161(1) (2000) 140–168.
52. P. Brown, G. Byrne, A. Hindmarsh, Vode: A variable-coefficient ode solver, SIAM J. Sci. Comput. 10(5) (1989) 1038–1051.

53. J. Chen, E. Hawkes, R. Sankaran, S. Mason, H. Im, Direct numerical simulation of ignition front propagation in a constant volume with temperature inhomogeneities I fundamental analysis and diagnostics, Combust. Flame 145 (2006) 128–144.

54. E. Hawkes, R. Sankaran, P. Pébay, J. Chen, Direct numerical simulation of ignition front propagation in a constant volume with temperature inhomogeneities II parametric study, Combust. Flame 145 (2006) 145–159.

55. D. Thévenin, O. Gicquel, J. de Charentenay, R. Hilbert, D. Veynante, Two- versus three-dimensional direct simulations of turbulent methane flame kernels using realistic chemistry, Proc. Combust. Inst. 29 (2002) 2031–2039.

56. B. Galmiche, F. Halter, F. Foucher, Effects of high pressure, high temperature and dilution on laminar burning velocities and markstein lengths of iso-octane/air mixtures, Combust. Flame 159 (2012) 3286–3299.

57. N. Peters, Laminar diffusion flamelet models in non-premixed turbulent combustion, Prog. Energy Combust. Sci. 10 (1984) 319–339.

58. P. Senecal, E. Pomraning, K. R. - Convergent Thinking, LLC, T. Briggs, C. Choi, R. McDavid, M. P. - Caterpillar, Inc., Multi-dimensional modeling of direct-injection Diesel spray liquid length and flame lift-off length using CFD and parallel detailed chemistry, SAE Paper 2003-01-1043 (2003).

59. J. Van Oijen, J. Lammers, L. De Goey, Modeling of complex premixed burner systems by using flamelet-generated manifolds, Combust. Flame 127 (2001) 2124–2134.

60. J. Van Oijen, A. Donini, R. Bastiaans, J. ten Thije Boonkkamp, L. De Goey, State-of-the-art in premixed combustion modeling using flamelet generated manifolds, Prog. Energy Combust. Sci. 57 (2016) 30–74.

61. C. Bekdemir, B. Somers, P. de Goey, DNS with detailed and tabulated chemistry of engine relevant igniting systems, Combust. Flame 161 (1) (2014) 210–221.

62. A. Klimenko, R. Bilger, Conditional moment closure for turbulent combustion, Prog. Energy Combust. Sci. 25 (1999) 595–687.

63. A. E. Sayed, M. Mortensen, J. Wen, Assessment of the presumed mapping function approach for the stationary laminar flamelet modelling of reacting double scalar mixing layers, Combust. Theory Model. 18 (4-5) (2014) 552–581.

64. G. Ribert, O. G. N. Darabiha, D. Veynante, Tabulation of complex chemistry based on self-similar behavior of laminar premixed flames., Combust. Flame 146 (2006) 649–664.